THESIS

GPU-ACCELERATED COMPUTATIONAL STUDY OF SELF-ASSEMBLED BLOCK COPOLYMERS

Submitted by

Vugar Hajizada

School of Biomedical and Chemical Engineering

In partial fulfillment of the requirements

For the Degree of Master of Science

Colorado State University

Fort Collins, Colorado

Summer 2026

Master's Committee:

Advisor: Qiang (David) Wang

Margarita Herrera-Alonso

Grzegorz Szamel

ABSTRACT

GPU-ACCELERATED COMPUTATIONAL STUDY OF SELF-ASSEMBLED BLOCK COPOLYMERS

This thesis uses GPU-accelerated theoretical calculations and molecular simulations of the dissipative particle dynamics chain (DPDC) model to study ordered phases of block copolymer melts. The DPDC model is a compressible model of discrete Gaussian chains interacting with the DPD non-bonded potential. It can be used in both particle-based simulations and self-consistent field (SCF) calculations, thus providing a stringent and quantitative assessment of the mean-field approximation inherent in the latter. This work has two parts: (1) parameter-free comparisons between Langevin dynamics (LD) and SCF results for ABC miktoarm star triblock terpolymers and (2) SCF study on the relative stability of Frank-Kasper (FK) phase of conformationally asymmetric diblock copolymers. For ABC stars, LD simulations were performed for several ordered phases including the three-layer lamellae (L_3), core-shell cylinders (C_3), hierarchical lamellae (HL), and two tiling patterns ([6^3] and [$8^2.4$]). LD simulation parameters were judiciously chosen, finite-size effects were carefully studied, and bulk periods were accurately determined from pressure-tensor analysis. The LD results were then directly compared with SCF calculations based on the same DPDC model. It is found that SCF theory overestimates the bulk periods and the changes in Helmholtz free energy, non-bonded internal energy, and chemical potential from the homopolymer melts, while underestimating the corresponding changes in entropy and pressure, for all phases solely due to the system fluctuations and correlations fully sampled in LD simulations but completely neglected in SCF theory. For diblock copolymers, 12

FK phases were considered: A15, σ, H, Z, pσ, C14, C15, zra-d, and 10-, 9-, 8-, and 6-layers. The Helmholtz free energy per chain and its energetic and entropic contributions were compared among these phases. It is found that the σ phase has the lowest free energy throughout the parameter range studied, with A15 being the closest competitor followed by H. The variations in the Helmholtz free energy and non-bonded internal energy curves of these FK phases are correlated with their average coordination number, and the relative stability of these FK phases is mainly controlled by their $A-B$ repulsion.

ACKNOWLEDGEMENTS

Financial support for this work was provided by the U.S. Department of Energy, Office of Basic Energy Sciences, Division of Materials Sciences and Engineering under Award No. DE-SC0023203, which is gratefully acknowledged. I want to thank Akshay Malik for developing an automated workflow of LD simulations, Juntong He for developing an extended and improved GPU version of PSCF, an open-source software package PSCF+, and Qiang Wang for his supervision and support during this project.

TABLE OF CONTENTS

LIST OF TABLES

LIST OF FIGURES

Figure 9. MATLAB visualizations of the converged SCF fields for (a) A15, (b) σ, (c) H, (d) Z, (e) pσ, and (f) C14 phases.

Figure 10. MATLAB visualizations of the converged SCF fields for (a) C15, (b) zra-d, (c) 6-layers, (d) 8-layers, (e) 9-layers, and (f) 10-layers phases.

Figure 11. Comparisons of (a) the dimensionless Helmholtz free energies per chain, $\beta f_c - \beta f_c^{\sigma}$, (b) the dimensionless internal energies per chain due to the *A*–*B* repulsion $\beta u_{c,\chi} - \beta u_{c,\chi}^{\sigma}$ and (c) those due to the system compressibility $\beta u_{c,\kappa} - \beta u_{c,\kappa}^{\sigma}$, and (d) the dimensionless entropies per chain $s_c^{\sigma}/k_B - s_c/k_B$ of FK phases calculated using PSCF+ for neat conformationally asymmetric diblock copolymer melts described by the DPDC model at $N = 20$, $f_A = 0.25$, $\epsilon = 4$, and $N/\kappa = 50$, with the σ phase taken as a reference.

1. INTRODUCTION

Block copolymers are macromolecules composed of two or more chemically distinct polymer blocks covalently connected to each other. Because chemically different blocks are usually thermodynamically incompatible, they tend to separate from one another. However, the covalent connection between the blocks prevents macrophase separation and instead leads to microphase separation into ordered nanostructures. Depending on molecular architecture, composition, chain conformational asymmetry, and segregation strength, block copolymers can self-assemble into many morphologies, including lamellae, cylinders, spheres, networks, and more complex low-symmetry ordered phases.[1]

Theoretical and computational methods are widely used to study block copolymer self-assembly because they allow the thermodynamics of competing ordered phases to be compared systematically. Self-consistent field (SCF) theory is one of the most common approaches for this purpose. In SCF theory, the many-chain interacting system is replaced by a single-chain problem in self-consistent fields, and the equilibrium structure is obtained by minimizing the mean-field Helmholtz free energy. SCF calculations are efficient for determining equilibrium density profiles, bulk periods, phase boundaries, and free-energy differences among ordered structures.[1,2] However, SCF theory is a mean-field theory and neglects fluctuations and correlations[3] in the system.

Particle-based simulations[4] provide a complementary approach because they explicitly include fluctuations and correlations. Methods such as molecular dynamics (MD), Langevin dynamics (LD), dissipative particle dynamics (DPD), and Monte Carlo (MC) simulations can be used to study both thermodynamic and structural properties of polymer systems[5]. However, particle-

based simulations also have limitations. They are performed in finite simulation boxes with periodic boundary conditions, and the simulation box can restrict the allowed period, orientation, and symmetry of an ordered morphology. In addition, simulations must be carefully equilibrated and sampled to obtain reliable averages and uncertainties. Therefore, quantitative comparison between particle-based simulations and SCF calculations requires careful treatment of simulation parameters, finite-size effects[6], and thermodynamic definitions.

Another important issue is the molecular model used in the comparison. Many SCF studies use the standard model of incompressible continuous Gaussian chains with Dirac delta-function non-bonded interactions. In contrast, particle-based simulations usually use discrete chains with finite-range soft interactions. If simulation and SCF calculations are performed with different models, then differences between their results can arise from both the different molecular models and the different theoretical approximations. A clearer comparison is possible when both methods use the same model.

In this thesis, the dissipative particle dynamics chain (DPDC) model is used as the common model for both LD simulations and SCF calculations.[1,7] The DPDC model is a compressible model of discrete Gaussian chains with the DPD non-bonded pair potential. Since the same model is used in both particle-based simulations and SCF calculations, the comparison between LD and SCF results does not require parameter fitting or mapping between different molecular models. This makes it possible to interpret differences between LD and SCF results mainly in terms of finite-size effects[6] in simulations and the fluctuations and correlations neglected by mean-field SCF theory.

The first part of the thesis focuses on ABC miktoarm star terpolymers[8]. An ABC miktoarm star terpolymer contains three chemically distinct blocks connected at a common junction. This

molecular architecture can form ordered structures that are more complex than those of linear diblock copolymers. In this work, LD simulations and SCF calculations are used to study several ordered ABC-star morphologies, including three-layer lamellae (L_3), hierarchical lamellae[9] (HL), core-shell cylinders (C_3), and the tiling patterns[10] $[6^3]$ and $[8^2.4]$.

For the ABC star terpolymer systems, the main goal is to perform a parameter-free comparison between LD simulations and SCF calculations using the same DPDC model. The LD simulation parameters are first validated using simpler systems for which exact values are known. Finite-size effects are then examined by comparing one-period and two-period simulation boxes. The bulk periods of the ordered phases are determined from the pressure tensor[11], and the resulting LD values are compared with the corresponding SCF predictions. Thermodynamic quantities, including the non-bonded internal energy, pressure, excess chemical potential, Helmholtz free energy, and entropy are also compared between LD and SCF calculations.

The second part of this thesis focuses on Frank-Kasper (FK) phases in conformationally asymmetric diblock copolymer melts. Interest in the self-assembly of linear and flexible diblock copolymer melts was renewed after the experimental discovery of the FK σ phase in 2010.[12] FK phases were first identified in metallic alloys and represent a class of complex ordered structures built from coordination polyhedra[13] with triangular faces. The four types of FK coordination polyhedra have coordination numbers 12, 14, 15, and 16.[13,14] Although 29 FK phases are known to date,[15] only a few of them have been found to be stable in diblock copolymer systems.

For neat diblock copolymer melts, only σ and A15 have been found to be stable FK phases.[12,16] Their stability over conventional spherical phases such as body-centered cubic and face-centered cubic spherical phases was first predicted by polymer self-consistent field calculations and later

confirmed experimentally.[17] The formation of these FK phases is closely connected to conformational asymmetry between the two blocks.[18] These predictions and experimental confirmations show the success of SCF theory in describing complex low-symmetry phases in block copolymer self-assembly.

Most SCF calculations of FK phases in neat diblock copolymer melts have used the standard model, which describes incompressible melts of continuous Gaussian chains with Dirac delta-function non-bonded interactions. In this model, the important parameters are the A-block volume fraction f_A, the conformational asymmetry ϵ, and the segregation strength χN. Previous SCF phase diagrams for neat diblock copolymer melts showed that σ and A15 are stable FK phases, whereas C14, C15, H, Z, and pσ are unstable.[7,19]

Many explanations for FK phase stability are based on structural features. In FK phases, the minority domains occupy Wigner-Seitz polyhedra of different sizes and shapes within the same unit cell. This differs from conventional spherical phases, where all minority domains are equivalent. Structural measures such as the sphericity of Wigner-Seitz polyhedra, the geometry of the A–B interface, and the packing frustration caused by nonspherical domains have been used to explain why FK phases can become favorable. However, the thermodynamically stable phase at a given state point is ultimately determined by the Helmholtz free energy. SCF theory is useful in this context because it provides the equilibrium volume-fraction fields, conjugate fields, Helmholtz free energy, and its energetic and entropic contributions.

With the stability mechanisms of FK phases over conventional spherical phases generally established, an important question is why some FK phases are stable while others are not. Previous FK stability analysis[19] showed that the relative stability among several FK phases is

dominated by the internal-energy density, corresponding to the repulsion between A and B blocks. It was also shown that variations of the Helmholtz free-energy and internal-energy curves are correlated with the average coordination number $\bar{z}$ of the Wigner-Seitz polyhedra. More specifically, FK phases with the same $\bar{z}$ tend to have nearly parallel free-energy and internal-energy curves, while phases with different $\bar{z}$ follow systematic trends according to their $\bar{z}$ values.

In this thesis, the relative stability of FK phases is studied using the DPDC model[7,20] rather than the standard model. The calculations are performed for neat conformationally asymmetric diblock copolymer melts at $N = 20, f_A = 0.25, \epsilon = 4$, and $N/\kappa = 50$, with χN varied from 25 to 40. The phases considered include 12 FK structures: A15, σ, H, Z, pσ, C14, C15, 10-layers, 9-layers, 8-layers, 6-layers, and zra-d structures. The σ phase is used as the reference phase. The Helmholtz free energy, A–B repulsion contribution, compressibility contribution, and entropy contribution are compared among these phases to determine their relative stability and to examine whether the trends reported in previous FK stability studies also appear in the DPDC model.

2. MODEL AND METHODS

2.1 Dissipative Particle Dynamics Chain (DPDC) Model

The dissipative particle dynamics chain (DPDC) model used in this work is a compressible model of discrete Gaussian chains with the DPD non-bonded pair potential. The same DPDC model is used for the Langevin dynamics (LD) simulations and the self-consistent field (SCF) calculations so that the two methods can be compared without introducing a mapping or fitting between different molecular models.

The system contains n block copolymer chains in a volume V at thermodynamic temperature T. Each chain contains N segments, and the average segment number density is $\rho_0 = \frac{nN}{V}$. For an ABC miktoarm star terpolymer, each chain contains three blocks, $P = A, B, C$, connected to a common joint segment J. The number of segments in block P is N_P, and

$$N = \sum_P N_P\,, \qquad f_P = \frac{N_P}{N}.$$

For the conformationally asymmetric diblock copolymer melts used in the Frank-Kasper (FK) phase calculations, each chain contains an A block and a B block, with

$$N = N_A + N_B, \qquad f_A = \frac{N_A}{N}, \qquad f_B = 1 - f_A.$$

In ABC stars, all segments except the joint segment J interact through non-bonded isotropic pair potentials. In diblock copolymer melts, all A and B segments interact through the same type of non-bonded pair potentials. The common excluded-volume interaction between all non-joint segments is described by

$$u^{\kappa}(r) = \frac{1}{\kappa\rho_0}\, u_0(r),$$

where κ is the generalized Helfand compressibility[21,22] parameter. In addition, unlike segments P and $P' \neq P$ repel each other through

$$u^{\chi}(r) = \frac{\chi}{\rho_0}\, u_0(r),$$

where the generalized Flory-Huggins parameter $\chi \geq 0$ controls the repulsion between chemically different blocks. Thus, the total non-bonded pair potential between two like non-joint segments is $u^{\kappa}(r)$, while that between two unlike non-joint segments is

$$u^{\kappa}(r) + u^{\chi}(r).$$

For the ABC star terpolymers considered here, the unlike interactions are symmetric, so the *A*–*B*, *B*–*C*, and *C*–*A* repulsions are characterized by the same χ.

The normalized DPD potential[23] is

$$\beta u_0(r) = \begin{cases} \frac{15}{2\pi\sigma^3}\left(1 - \frac{r}{\sigma}\right)^2, & r < \sigma, \\ 0, & r \geq \sigma, \end{cases}$$

with the normalization

$$4\pi \int_0^{\infty} dr r^2\, \beta u_0(r) = 1.$$

Here $\beta \equiv 1/(k_B T), k_B$ is the Boltzmann constant, T is the thermodynamic temperature, and σ is the cut-off distance of the DPD potential (taken as the unit of length).

The chain connectivity is described by the discrete Gaussian chain model.[1,7] Adjacent bonded segments interact through the dimensionless bonding potential

$$\beta u^b(r) = \frac{3r^2}{2b^2} - \frac{3}{2}\ln\left[\frac{3}{2\pi(\frac{b}{\sigma})^2}\right],$$

with

$$4\pi\int_0^\infty drr^2\ \exp\Big(-\beta u^b(r)\Big) = 1,$$

where r is the distance between two bonded segments and b is the effective bond length.

The molecular parameters used for the LD simulation part of our work are

$$N = 20, \qquad \rho_0\sigma^3 = 3, \qquad \frac{b}{\sigma} = \frac{\sqrt{3}}{2}, \qquad \frac{N}{\kappa} = 50.$$

For conformationally asymmetric diblock copolymer melts, the conformational asymmetry is defined as

$$\epsilon = \left(\frac{b_A}{b_B}\right)^2,$$

where b_A and b_B are the effective bond lengths of the *A* and *B* blocks. In the FK phase calculations of this work, the main parameter set is

$$\epsilon = 4, \qquad f_A = 0.25, \qquad N = 20, \qquad \frac{N}{\kappa} = 50,$$

with χN varied from 25 to 40.[7] In this parameter set, $b_A/b_B = 2$.

2.2 Langevin Dynamics Simulations

LD simulations are used for the ABC miktoarm star terpolymer part of this thesis. The simulations are performed using HOOMD-blue[24] within the automated workflow developed by our group. The conservative forces are obtained from the bonded and non-bonded DPDC pair potentials described in Sec. 2.1. In the LD simulations, the force acting on segment i is written as

$$\beta\sigma\mathbf{F}_i = \sum_{j\neq i} \beta\,\sigma\mathbf{F}_{ij}^{C} - \gamma\sqrt{\beta m}\,\mathbf{v}_i + \sqrt{2\gamma}\,\boldsymbol{\xi}_i,$$

where $\mathbf{F}_{ij}^{C}$ is the conservative force exerted on segment i by segment j, m is the mass of each segment, $\mathbf{v}_i$ is the velocity of segment i, $\gamma = 1$ is the dimensionless friction parameter, and $\boldsymbol{\xi}_i$ is a Gaussian random variable with zero mean and unit variance. The time unit is $\tau \equiv \sqrt{\beta m}\,\sigma$ and a timestep of $\delta t = 0.01\tau$ is used. This value was determined by performing simulations of ideal linear chains and comparing ensemble-averaged quantities such as the dimensionless temperature, mean-square chain end-to-end distance, internal energy, and pressure with their exact values.

For each ordered phase, the initial particle configuration for the LD simulation was generated from the corresponding converged SCF solution. The SCF solution therefore provided an initial configuration consistent with the target morphology, which was then equilibrated using LD before thermodynamic quantities were calculated.

Each simulation case is divided into a pilot run and a production run. In the pilot run, the pyMSER[25] method is used to determine the equilibration time t_{eq}. Let t_{out} be the time interval used to collect each sample and let M be the number of samples collected after equilibration in the pilot run. For a sampled quantity A, the ensemble average is

$$\bar{A} = \frac{1}{M}\sum_{i=1}^{M} A_i,$$

where A_i is the value of A in the ith sample. The statistical uncertainty is estimated with the sample correlation taken into account as[4]

$$\sigma_A^2 = \frac{g_A}{M-1}\left(\overline{A^2} - \bar{A}^2\right),$$

where g_A is the statistical inefficiency estimated from the correlation function. The pilot run is used to estimate g_A and to choose an appropriate sampling interval for the production run so that the collected samples are nearly uncorrelated.

The ABC star phases studied by LD simulations include lamellae L_3, core-shell cylinders C_3 and the [6^3] phase, squarely packed cylinders [8^2.4], and hierarchical lamellae HL. For each morphology, simulations are performed in periodic boxes compatible with the target symmetry. One-period and two-period boxes are compared to examine the effect of imposed periodicity and finite system size on thermodynamic quantities and morphology.

2.3 Bulk Period and Finite-Size Analysis in LD Simulations

For ordered block copolymer phases, the simulation box[26] restricts the allowed periodicity of the structure. This restriction can affect both the morphology and the measured thermodynamic quantities. Therefore, the bulk period and finite-size effects[6] must be treated carefully before comparing different phases or comparing LD simulations with SCF calculations.

Based on our recent work[11], for one-dimensional and two-dimensional ordered structures, the bulk period L_0 is determined from the pressure tensor[11] using

$$\Delta_D \equiv \beta\sigma^3 \left[\left(P_{xx} - P_{yy}\right)^2 + \left(P_{yy} - P_{zz}\right)^2 + (P_{xx} - P_{zz})^2 \right],$$

where P_{dd} is the dd-component of the pressure tensor[11] calculated from the virial. The bulk period is estimated as the value of the period L that minimizes Δ_D. Simulations are performed for several nearby values of L, and the minimum is obtained by fitting the lowest data points to a parabola.

For three-dimensional ordered structures[27], the pressure-tensor method does not directly apply. In that case, the bulk period is determined by minimizing the dimensionless excess Helmholtz free energy per chain,

$$\beta f_c^{ex} = \beta\mu^{ex} - \frac{N\beta P^{ex}}{\rho_0},$$

where μ^{ex} is the excess chain chemical potential and P^{ex} is the excess pressure. The excess chemical potential is computed using Rosenbluth sampling[4], and the excess pressure is calculated from the virial.

Finite-size effects are examined by comparing results obtained in one-period and two-period simulation boxes. The main quantities compared include the non-bonded internal energy per chain, pressure tensor, excess chemical potential, and Helmholtz free energy per chain. This analysis is used to determine whether a one-period box is sufficient for a given ABC star phase or whether a two-period box is needed to approximate the bulk behavior.

2.4 Self-Consistent Field Calculations Using PSCF+

SCF calculations are performed using PSCF+, an extended and improved version of PSCF[2] for unit-cell calculations of block copolymer self-assembly. PSCF+ has been extended to include the

DPDC model. For a specified chain architecture, value of χN, and ordered-phase symmetry, PSCF+ solves for the equilibrium volume-fraction fields $\phi_P(r)$ and conjugate fields $\omega_P(r)$, where P denotes the segment type.

For a melt of linear diblock copolymers described by the DPDC model, each chain contains an A block followed by a B block. The microscopic segment densities are defined as

$$\hat{\rho}_A(\mathbf{r}) = \sum_{k=1}^{n} \sum_{s=1}^{N_A} \delta\left(\mathbf{r} - \mathbf{R}_{k,s}\right),$$

and

$$\hat{\rho}_B(\mathbf{r}) = \sum_{k=1}^{n} \sum_{s=N_A+1}^{N} \delta\left(\mathbf{r} - \mathbf{R}_{k,s}\right),$$

where $\mathbf{R}_{k,s}$ is the position of segment s on chain k, n is the number of chains, $N = N_A + N_B$, and $N_A/N = f_A$.

The configurational canonical-ensemble partition function of the system can be written as

$$Z = \prod_{k=1}^{n} \sum_{s=1}^{N} \int d\mathbf{R}_{k,s} \exp\left[- \sum_{k=1}^{n} \sum_{s=1}^{N-1} \beta\, u_{k,s}^{b} - \beta \mathcal{H}^{nb}[\hat{\rho}_A, \hat{\rho}_B] \right],$$

where $u_{k,s}^{b}$ is the bonding potential between adjacent segments s and $s+1$ on chain k, and $\mathcal{H}^{nb}$ is the non-bonded Hamiltonian. For the DPDC model, the non-bonded Hamiltonian can be written as

$$\mathcal{H}^{nb} = \mathcal{H}^{\kappa} + \mathcal{H}^{\chi} - \frac{nN}{2\kappa\rho_0} u_0(0),$$

where the compressibility contribution is

$$\mathcal{H}^{\kappa} = \frac{1}{2\kappa\rho_0}\int d\mathbf{r}\int d\mathbf{r}'\,[\hat{\rho}_A(\mathbf{r}) + \hat{\rho}_B(\mathbf{r})]u_0(|\mathbf{r}-\mathbf{r}'|)[\hat{\rho}_A(\mathbf{r}') + \hat{\rho}_B(\mathbf{r}')],$$

and the *A*–*B* repulsion contribution is

$$\mathcal{H}^{\chi} = \frac{\chi}{\rho_0}\int d\mathbf{r}\int d\mathbf{r}'\,\hat{\rho}_A(\mathbf{r})u_0(|\mathbf{r}-\mathbf{r}'|)\hat{\rho}_B(\mathbf{r}').$$

Here $\rho_0 = nN/V$ is the average segment number density, κ is the generalized Helfand compressibility parameter, χ is the generalized Flory-Huggins parameter, and $u_0(r)$ is the normalized DPD potential. The final term in $\mathcal{H}^{nb}$ subtracts the self-interactions.

To transform the particle model to a field model, normalized density fields $\phi_A(\mathbf{r})$ and $\phi_B(\mathbf{r})$, together with their conjugate fields $\omega_A(\mathbf{r})$ and $\omega_B(\mathbf{r})$, are introduced through the identity

$$1 = \prod_{j=A,B}\int \mathcal{D}\phi_j\,\mathcal{D}\omega_j \exp\{\int d\mathbf{r}\,\omega_j(\mathbf{r})[\rho_0\phi_j(\mathbf{r}) - \hat{\rho}_j(\mathbf{r})]\}.$$

After inserting this identity into the partition function and rescaling variables, the partition function becomes

$$Z = \int \mathcal{D}\phi_A\,\mathcal{D}\omega_A\,\mathcal{D}\phi_B\,\mathcal{D}\omega_B \exp\{-n\beta f_c[\phi_A,\phi_B,\omega_A,\omega_B]\}.$$

The dimensionless SCF free-energy functional per chain is

$$\beta f_c = \beta f_{c,\chi} + \beta f_{c,\kappa} - W - \ln Q,$$

where

$$\beta f_{c,\chi} = \frac{\chi N}{V}\int d\mathbf{r}\int d\mathbf{r}'\,\phi_A(\mathbf{r})\beta u_0(|\mathbf{r}-\mathbf{r}'|)\phi_B(\mathbf{r}'),$$

$$\beta f_{c,\kappa} = \frac{N}{2\kappa V}\int d\mathbf{r}\int d\mathbf{r}'\,[\phi_A(\mathbf{r}) + \phi_B(\mathbf{r})]\beta u_0(|\mathbf{r}-\mathbf{r}'|)[\phi_A(\mathbf{r}') + \phi_B(\mathbf{r}')],$$

and

$$W = \frac{1}{V}\int d\mathbf{r}\,[\omega_A(\mathbf{r})\phi_A(\mathbf{r}) + \omega_B(\mathbf{r})\phi_B(\mathbf{r})].$$

Here Q is the normalized single-chain partition function in the external fields.

In PSCF+, the SCF equations are obtained by requiring the functional to be stationary with respect to the density and conjugate fields,

$$\frac{\delta\beta f_c}{\delta\phi_j(\mathbf{r})} = 0,$$

and

$$\frac{\delta\beta f_c}{\delta\omega_j(\mathbf{r})} = 0, \qquad j = A, B.$$

In Fourier space, the conjugate-field equations are

$$\widehat{\omega}_A(\mathbf{k}) = \beta\hat{u}_0(k)\left[\frac{N}{\kappa}\hat{\phi}_A(\mathbf{k}) + \left(\frac{N}{\kappa} + \chi N\right)\hat{\phi}_B(\mathbf{k})\right],$$

and

$$\widehat{\omega}_B(\mathbf{k}) = \beta\hat{u}_0(k)\left[\frac{N}{\kappa}\hat{\phi}_B(\mathbf{k}) + \left(\frac{N}{\kappa} + \chi N\right)\hat{\phi}_A(\mathbf{k})\right].$$

The volume-fraction fields are calculated from the forward chain propagator $q_s(\mathbf{r})$ and the backward chain propagator $q^{\dagger}_{N-s+1}(\mathbf{r})$ as

$$\phi_A(\mathbf{r}) = \frac{\exp[\omega_A(\mathbf{r})/N]}{N\hat{q}_N(\mathbf{k}=0)/V}\sum_{s=1}^{N_A} q_s(\mathbf{r})q^{\dagger}_{N-s+1}(\mathbf{r}),$$

and

$$\phi_B(\mathbf{r}) = \frac{\exp[\omega_B(\mathbf{r})/N]}{N\hat{q}_N(\mathbf{k}=0)/V}\sum_{s=N_A+1}^{N} q_s(\mathbf{r})q^{\dagger}_{N-s+1}(\mathbf{r}).$$

The forward propagator satisfies the Chapman-Kolmogorov equation.[21,28] Starting from the A end of the chain,

$$q_1(\mathbf{r}) = \exp[-\omega_A(\mathbf{r})/N],$$

and

$$q_{s+1}(\mathbf{r}) = \exp[-\omega_A(\mathbf{r})/N]\int d\mathbf{r}'\,\Phi_A(|\mathbf{r}-\mathbf{r}'|)q_s(\mathbf{r}'), \qquad s = 1, \ldots, N_A - 1,$$

while for the B block,

$$q_{s+1}(\mathbf{r}) = \exp[-\omega_B(\mathbf{r})/N]\int d\mathbf{r}'\,\Phi_B(|\mathbf{r}-\mathbf{r}'|)q_s(\mathbf{r}'), \qquad s = N_A, \ldots, N - 1.$$

The backward propagator is defined analogously by starting from the B end of the chain. The normalized bond transition probability for block P is

$$\Phi_P(\mathbf{b}) = \left(\frac{3}{2\pi b_P^2}\right)^{3/2}\exp\left[-\frac{3|\mathbf{b}|^2}{2b_P^2}\right], \qquad P = A, B,$$

where b_P is the effective bond length of block P. For conformationally asymmetric diblock copolymers, $b_A \neq b_B$, and the conformational asymmetry is $\epsilon = (b_A/b_B)^2$.

After the SCF equations are solved, the minimized free energy is obtained from the converged fields and density profiles. Using the notation of the propagator formulation, it can be written as

$$\beta f_c = -I_\kappa - I_\chi - \ln\left[\frac{\hat{q}_N(\mathbf{k}=0)}{V}\right],$$

where

$$I_\kappa = \frac{1}{V}\int \frac{d\mathbf{k}}{(2\pi)^3}\,\frac{N}{2\kappa}\left[\hat{\phi}_A(\mathbf{k}) + \hat{\phi}_B(\mathbf{k})\right]\beta\hat{u}_0(k)\left[\hat{\phi}_A(-\mathbf{k}) + \hat{\phi}_B(-\mathbf{k})\right],$$

and

$$I_\chi = \frac{1}{V}\int \frac{d\mathbf{k}}{(2\pi)^3}\,\chi N\hat{\phi}_A(\mathbf{k})\beta\hat{u}_0(k)\hat{\phi}_B(-\mathbf{k}).$$

This expression gives the dimensionless mean-field Helmholtz free energy per chain at the SCF saddle point. The minimized value of βf_c, together with the internal-energy and entropy is used to compare the relative stability of candidate FK phases.

The unit-cell size and shape are adjusted to minimize the dimensionless Helmholtz free energy per chain, βf_c. The minimized free energy and its energetic and entropic components are then used for comparison between phases. For the ABC star part of this thesis, SCF calculations provide the mean-field reference for the LD simulation results. Since the LD simulations and SCF calculations use the same DPDC model, their differences reflect the effect of fluctuations and correlations that are included in LD simulations but neglected in SCF theory.

For the FK part of this thesis, PSCF+ is used to calculate the relative stability of candidate FK phases in neat conformationally asymmetric diblock copolymer melts. The FK phases include $\mathtt{A15}, \sigma, \mathtt{H}, \mathtt{Z}, \mathrm{p}\sigma, \mathtt{C14}, \mathtt{C15}$, 10-layers, 9-layers, 8-layers, 6-layers, and zra-d.[29]

For each phase and each value of χN, the SCF equations and the unit-cell optimization equations are solved until the convergence criterion is satisfied. The satisfactory grid settings are

determined for the present calculations by increasing the spatial resolution until the PSCF+ convergence and free-energy accuracy are adequate for comparing the small free-energy differences among FK phases.

2.5 Thermodynamic Quantities from SCF Calculations

For the DPDC model, the internal energy contains a contribution from the system compressibility and a contribution from repulsion between unlike blocks. For a diblock copolymer melt, the *A*–*B* repulsion contribution is

$$\beta u_{c,\chi} = \frac{\chi N}{V} \int d\mathbf{r} \int d\mathbf{r}' \, \phi_A(\mathbf{r}) \, \beta u_0(|\mathbf{r} - \mathbf{r}'|) \, \phi_B(\mathbf{r}'),$$

and the compressibility contribution is

$$\beta u_{c,\kappa} = \frac{N}{2\kappa V} \int d\mathbf{r} \int d\mathbf{r}' \, [\phi_A(\mathbf{r}) + \phi_B(\mathbf{r})] \beta u_0(|\mathbf{r} - \mathbf{r}'|) [\phi_A(\mathbf{r}') + \phi_B(\mathbf{r}')].$$

The total dimensionless internal energy per chain is

$$\beta u_c = \beta u_{c,\chi} + \beta u_{c,\kappa}.$$

For an ABC star terpolymer with symmetric unlike interactions, the corresponding unlike-block contribution is

$$\beta u_{c,\chi} = \frac{\chi N}{V} \sum_{P<P'} \int d\mathbf{r} \int d\mathbf{r}' \, \phi_P(\mathbf{r}) \, \beta u_0(|\mathbf{r} - \mathbf{r}'|) \, \phi_{P'}(\mathbf{r}'),$$

where (P, P') runs over (A, B), (B, C), and (C, A). The compressibility contribution is

$$\beta u_{c,\kappa} = \frac{N}{2\kappa V} \int d\mathbf{r} \int d\mathbf{r}' \left[\sum_P \phi_P(\mathbf{r}) \right] \beta u_0(|\mathbf{r} - \mathbf{r}'|) \left[\sum_P \phi_P(\mathbf{r}') \right].$$

The dimensionless entropy per chain is obtained from

$$\frac{s_c}{k_B} = \beta u_c - \beta f_c.$$

For the FK phase comparisons, the σ phase is used as the reference. For any phase X, the relative Helmholtz free energy, internal energy, and entropy are defined as

$$\Delta(\beta f_c)^{\mathrm{X}} = \beta f_c^{\mathrm{X}} - \beta f_c^{\sigma},$$

$$\Delta(\beta u_c)^{\mathrm{X}} = \beta u_c^{\mathrm{X}} - \beta u_c^{\sigma},$$

and

$$\Delta\left(\frac{s_c}{k_B}\right)^{\mathrm{X}} = \frac{s_c^{\mathrm{X}}}{k_B} - \frac{s_c^{\sigma}}{k_B}.$$

A phase with a lower value of βf_c is thermodynamically more stable at the same parameter set. The decomposition into internal energy and entropy is used to determine whether the relative stability is mainly energetic, entropic, or due to a balance between the two.

For LD-SCF comparisons of ABC star phases, differences from the homopolymer melt at the same N/κ and $\chi N = 0$ are used:

$$\Delta f_c = f_c(N/\kappa, \chi N) - f_c(N/\kappa, 0),$$

with analogous definitions for internal energy, pressure, chemical potential, and entropy.

2.6 Coordination-Number-Based Quantities for FK Phases

The FK structures are analyzed using the coordination numbers of their Wigner-Seitz polyhedra. For an FK phase, the average coordination number is

$$\bar{z} = \frac{\sum_z n_z \, z}{\sum_{z'} n_{z'}},$$

where $z = 12, 14, 15, 16,$ and n_z is the number of Wigner-Seitz polyhedra with coordination number z in the unit cell.

To connect the geometry of an FK phase to its thermodynamics, energy-weighted coordination numbers calculations are also important.[19] The internal-energy-weighted average coordination number is

$$\bar{z}_u = \frac{\sum_z z \; u_{c,z}}{\beta u_c},$$

where $u_{c,z}$ is the internal-energy contribution from all Wigner-Seitz polyhedra with coordination number z. The Helmholtz-free-energy-weighted average coordination number is

$$\bar{z}_f = \frac{\sum_z z \; f_{c,z}}{\beta f_c},$$

where $f_{c,z}$ is the Helmholtz free-energy contribution from all Wigner-Seitz polyhedra with coordination number z. In this work, $\bar{z}_u$ and $\bar{z}_f$ calculations for the FK phases studied in the DPDC model are not completed yet and considered as a future direction to extend this study.

3.1 LD Simulations and SCF Comparisons of ABC Star Terpolymer Phases

3.1.1 Determination of LD simulation parameters

Before we used LD simulations to study ABC star terpolymers, to determine the appropriate timestep δt in units of $\tau \equiv \sqrt{\beta m}\sigma$ for our LD simulations, we simulated a system of ideal linear chains of N=10 (*i.e.*, N/κ=χN=0), for which we had the exact results of mean-square chain end-to-end distance $R_e^{\,2} = 3(N-1)\sigma^2/4$, dimensionless internal energy per chain (excluding the ideal-gas contribution) βu_c=3(N–1)/2, and dimensionless pressure $\beta P/\rho_0 = 1/N$.

Figure 1 below shows how these ensemble-averaged quantities, including the dimensionless temperature $\tilde{T} \equiv \left(\beta m/3nN\right)\sum_{i=1}^{nN} \mathbf{v}_i^{\,2}$, vary with δt.

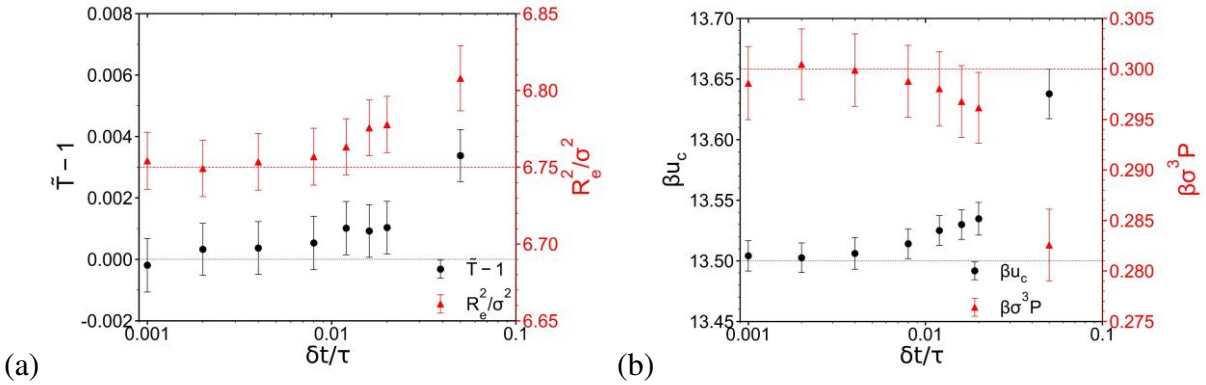

(a) (b)

Figure 1. Semi-logarithmic plots of the ensemble-averaged (a) dimensionless temperature $\tilde{T}$ (left axis) and mean-square chain end-to-end distance R_e^2 (right axis) and (b) internal energy per chain excluding the ideal-gas contribution u_c (left axis) and pressure P (right axis) obtained from our LD simulations of ideal linear chains each having N=10 segments with various timestep δt, where the horizontal lines mark their exact values.

Based on these results, we chose δt=0.01 τ in our subsequent simulations, which led to a relative error of ~0.2% for $\tilde{T}$, ~0.1% for R_e^2 and u_c, and ~0.5% for P in this case. Similar results were found for other systems (*e.g.*, homopolymers of N=10 and n=300 at N/κ=50, where in addition to the same trends for above quantities, we found that βf_c increases with increasing δt; and lamellae formed by linear symmetric DBCs of N=10 and n=68 at N/κ=50 and χN=30π, where in addition to the same trends for above quantities, we observed that βf_c increases and $\beta\mu^{ex}$ decreases with increasing δt.).

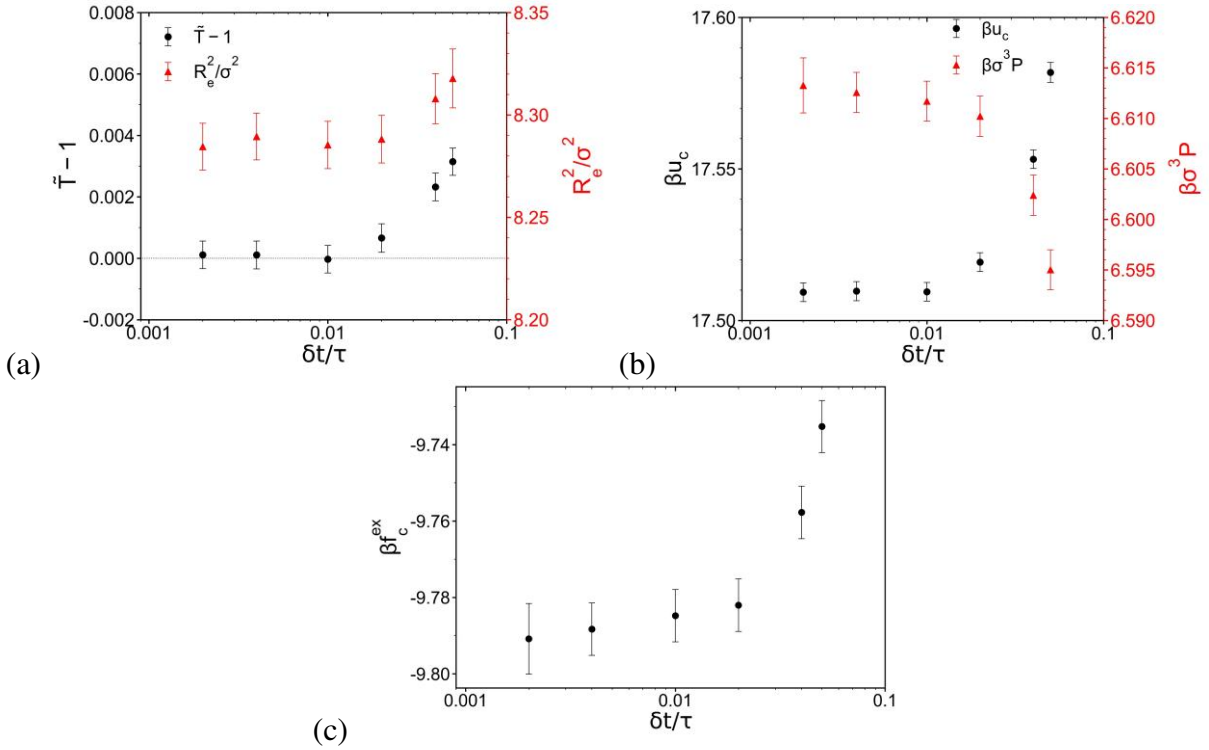

Figure 2. Semi-logarithmic plots of the ensemble-averaged (a) dimensionless temperature $\tilde{T}$ (left axis) and mean-square chain end-to-end distance R_e^2 (right axis), (b) internal energy per chain excluding the ideal-gas contribution u_c (left axis) and pressure P (right axis), and (c) Helmholtz free energy per chain βf_c obtained from our LD simulations of homopolymer chains each having N=10 segments with various timestep δt.

The production-run averages and error bars reported above were obtained using the pilot-run and sampling procedure described in Sec. 2.2. This procedure determines the equilibration time, estimates the statistical inefficiency of sampled quantities, and selects a sampling interval for the production run so that the collected samples are nearly uncorrelated.

We also examined the finite-size effects. Taking lamellae (L) formed by linear symmetric DBCs of N=10 at χN=30π as an example, Figure 3 shows that the internal energy per chain due to the non-bonded interactions u_c^{nb}, pressure P, excess chemical potential μ^{ex}, and Helmholtz free energy per chain f_c all vary approximately linearly with 1/V, where V denotes the volume of a cubic simulation box containing n_p periods of lamellae at the same period L.

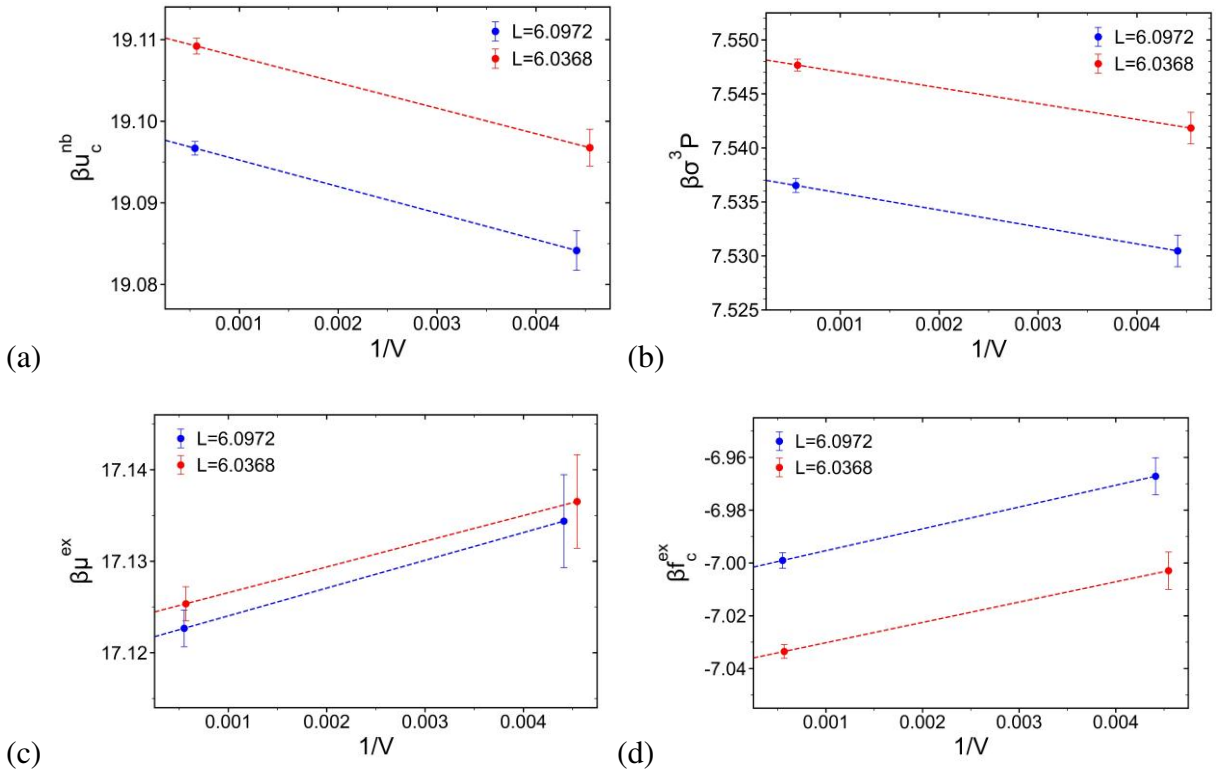

Figure 3. The dependence of (a) internal energy per chain due to the non-bonded interactions βu_c^{nb}, (b) pressure P, (c) excess chemical potential $\beta\mu^{ex}$, and (d) Helmholtz free energy per chain βf_c on $1/V$ at the periods L=6.0972 and L=6.0368 highlighted as blue and red respectively, where V denotes the volume of a cubic simulation box containing n_p periods of lamellae formed by linear symmetric DBCs of N=10 at χN=30π.

Based on these results, we took n_p=2 in our subsequent simulations of ABC star terpolymers, where the finite-size effects are negligible within the accuracy of our simulation results. Similar results were obtained for other phases including hierarchical lamellae (HL), three-layer lamellae (L_3), and hexagonally packed cylinders with honeycomb tiling pattern known as [6^3] shown in Figures 4, 5, and 6, correspondingly.

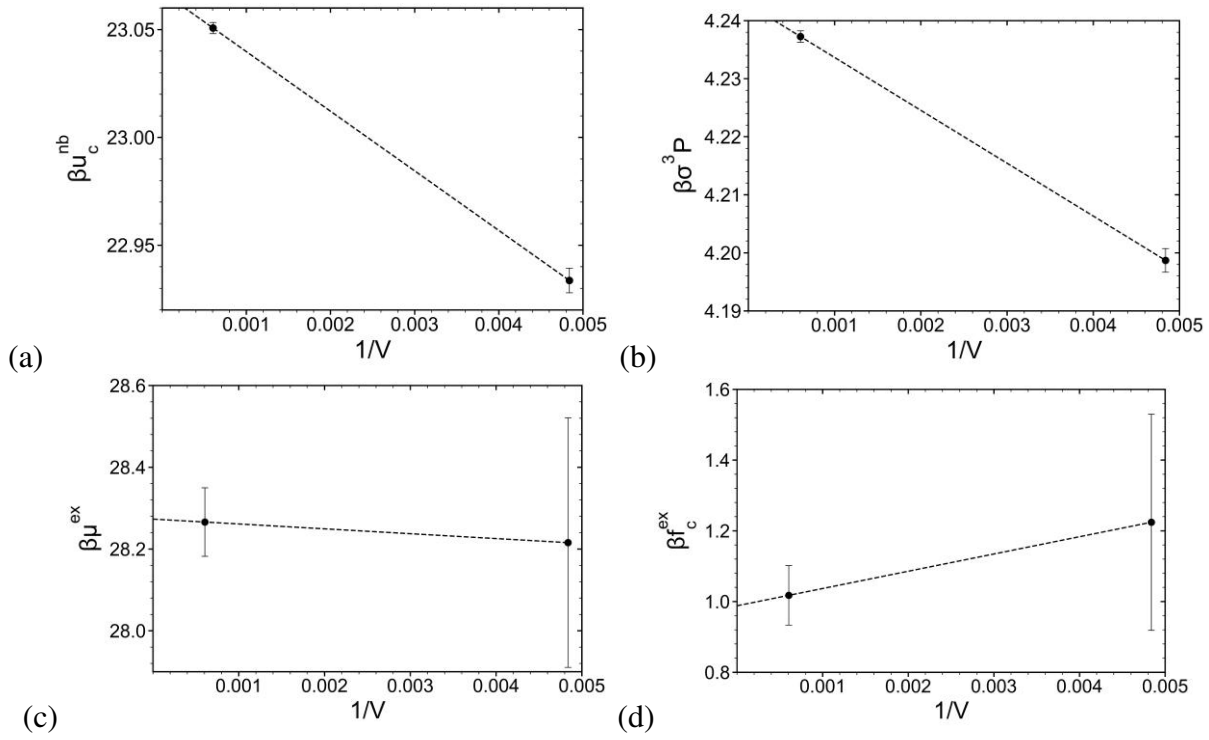

Figure 4. The dependence of (a) internal energy per chain due to the non-bonded interactions βu_c^{nb}, (b) pressure P, (c) excess chemical potential $\beta\mu^{ex}$, and (d) Helmholtz free energy per chain βf_c on $1/V$ at the same period L, where V denotes the volume of a cubic simulation box containing n_p periods of HL formed by ABC stars of N=20 at χN=100.

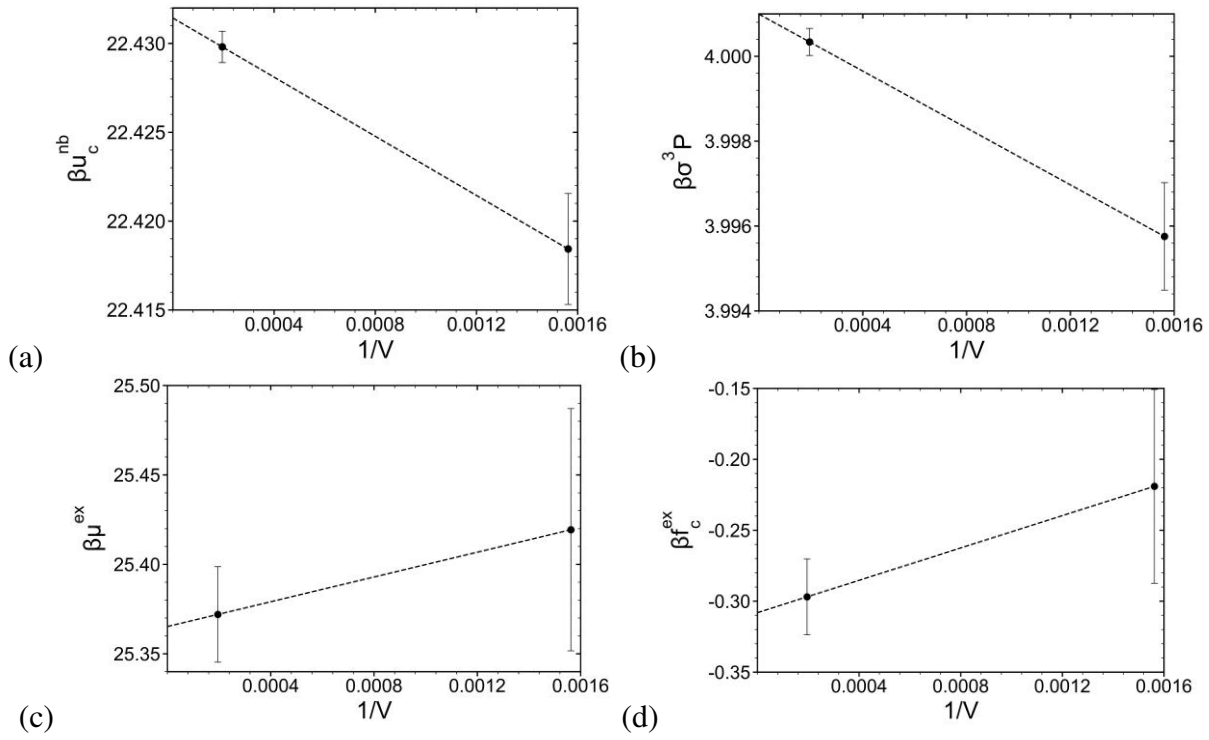

Figure 5. The dependence of (a) internal energy per chain due to the non-bonded interactions βu_c^{nb}, (b) pressure P, (c) excess chemical potential $\beta\mu^{ex}$, and (d) Helmholtz free energy per chain βf_c on $1/V$ at the same period L, where V denotes the volume of a cubic simulation box containing n_p periods of L_3 formed by ABC stars of N=20 at χN=100.

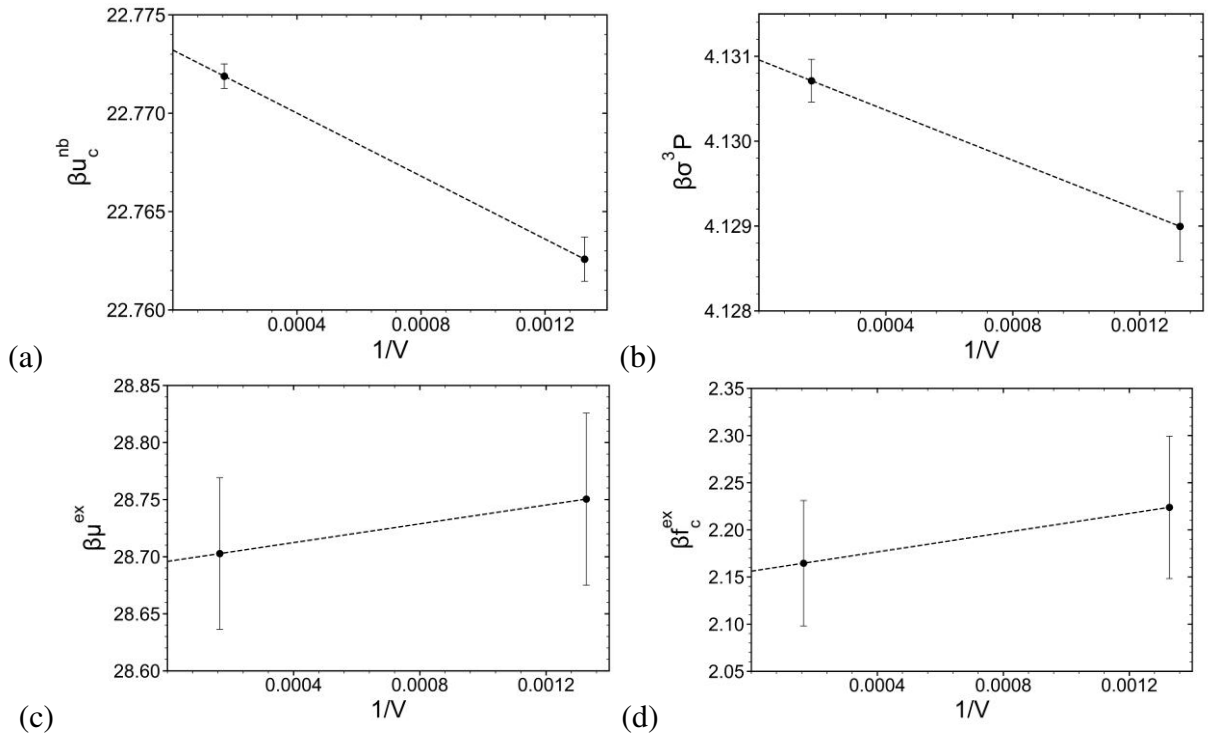

Figure 6. The dependence of (a) internal energy per chain due to the non-bonded interactions βu_c^{nb}, (b) pressure P, (c) excess chemical potential $\beta\mu^{ex}$, and (d) Helmholtz free energy per chain βf_c on $1/V$ at the same period L, where V denotes the volume of a cubic simulation box containing n_p periods of [6^3] formed by ABC stars of N=20 at χN=100.

For squarely packed cylinders [8^2.4] and core-shell cylinders (C_3), we were only able to simulate 2 and 1 periods of corresponding structure, since the simulation of 1 period of [8^2.4] failed to equilibrate and the 2 periods of C_3 experienced multiple orientations of cylinders in the simulation box.

3.1.2 LD-SCF Results Comparison for ABC Star Ordered Phases

As shown in a previous paper by our group, the bulk period L_0 of a 1D or 2D ordered structure can be found from the elements of the pressure tensor[11]. Figure 7 shows how

$$\Delta_D \equiv \beta\sigma^3\left[\left(P_{xx}-P_{yy}\right)^2+\left(P_{yy}-P_{zz}\right)^2+\left(P_{xx}-P_{zz}\right)^2\right],$$

where P_{dd} (d=x,y,z) denotes the dd-component of the pressure tensor calculated from the virial in our LD simulations, varies with L for L_3, HL, C_3, [6^3], and [8^2,4] structures formed by ABC stars of N=20 at χN=100; from the three lowest data points, we estimate the bulk period L_0/σ as the location of the minimum of the parabolic curve passing through these points. Table 1 lists the so-

Table 1. Parameter-free comparison of bulk period L_0 of ordered phases formed by the DPDC model of ABC stars obtained from LD simulations and SCF calculations in this work, where $\rho_0\sigma^3$=3, $b/\sigma = \sqrt{3}/2$, χN=100, and N/κ=50.

#	Phase	N	f_A	f_B	L_0/σ	$L_{0,SCF}/L_0$
1	L_3	20	11/20	2/5	8.6813±0.0039	1.085
2	HL	20	11/20	1/4	7.598±0.011	1.047
3	C_3	20	7/10	1/4	8.965±0.053	1.081
4	[6^3]	20	2/5	3/10	7.6052±0.0032	1.074
5	[8^2.4]	20	2/5	2/5	7.8697±0.0052	1.08

obtained L_0 for various tiling patterns. L_3 is parallel to one of the faces in cubic simulation boxes of side length 2L. For C_3, [6^3], and [8^2,4] which consist of cylinders with even-sided polygonal cross sections, we used a rectangular prism simulation box of side lengths $L_y = L_z = L_x/p \equiv L_b$ with the cylinders oriented along the y- or z-direction and $p = \sqrt{3}$ for C_3, [6^3], and 1 for [8^2.4]. Here L_0 denotes the smallest distance between cylinders formed by the majority (A) component for [6^3] and [8^2,4] and non-majority (B and C) components for C_3. We also used a rectangular prism simulation box of side lengths $L_y = L_z = L_x/p \equiv L_b$ with the lamellae perpendicular to the x-direction for the HL structure and p≈1.4293 obtained from SCF calculations, where L_0 denotes the smallest distance between lamellae formed by the majority (A) component.

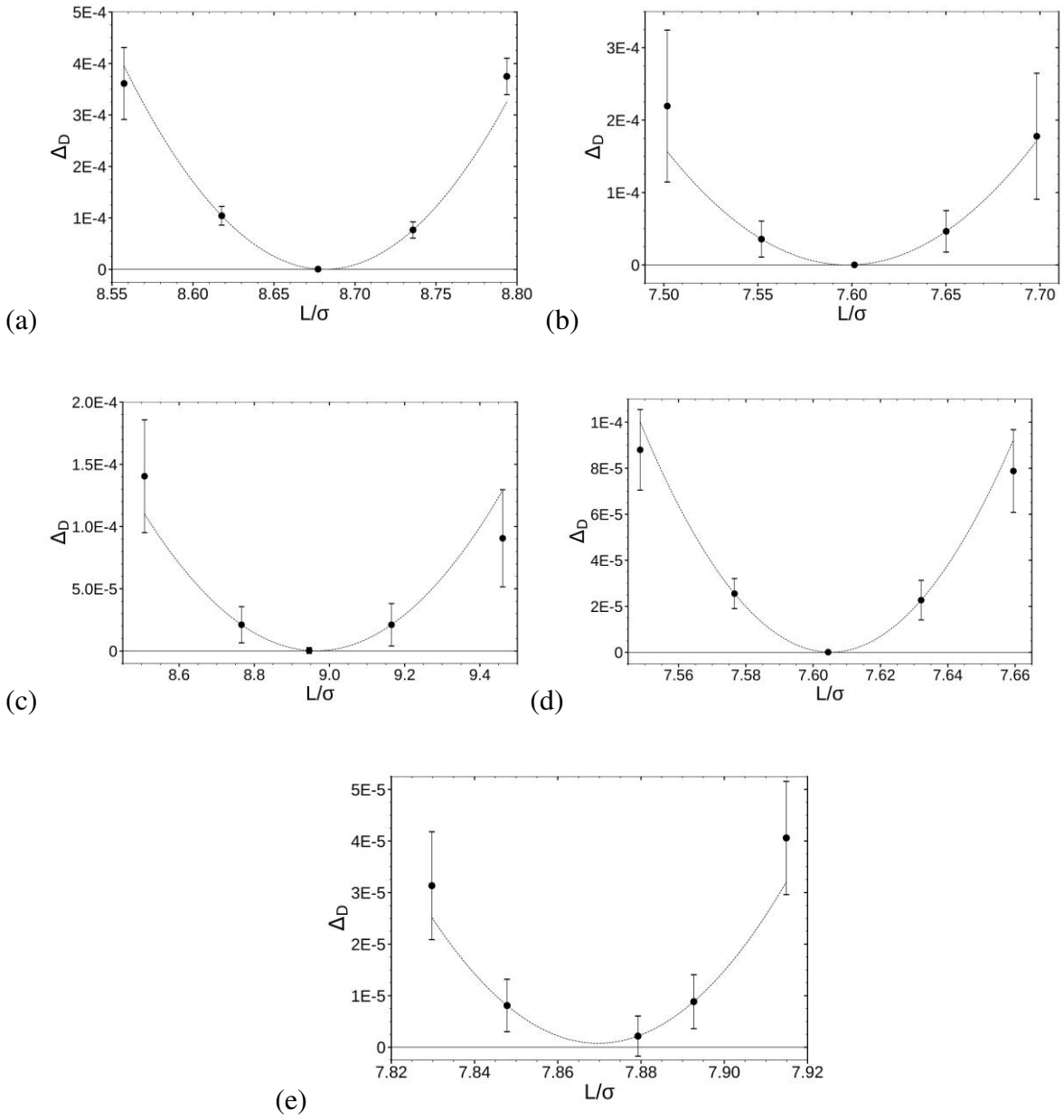

Figure 7. The bulk period L_0/σ as the location of the minimum of the parabolic curve passing through the three lowest data points in the Δ_D vs. L plots for (a) L_3, (b) HL, (c) C_3, (d) $[6^3]$, and (e) $[8^2,4]$ structures formed by ABC stars of N=20 at χN=100.

The [12.6.4] tiling pattern was also considered for LD simulations. Although the simulation was initialized from the corresponding converged SCF solution, the [12.6.4] morphology was not maintained during equilibration and instead transformed into the hierarchical lamellar (HL). Therefore, [12.6.4] was not included in the subsequent quantitative LD-SCF comparisons.

Since the same DPDC model is used in both our LD simulations and SCF calculations, there is no parameter-fitting and any difference between them is solely due to the mean-field approximation inherent in the latter that neglects the system fluctuations and correlations. Table 1 compares the bulk period L_0^{SCF} obtained from our SCF calculations using PSCF+ to L_0 for the various phases studied in this work.

Table 2. Parameter-free comparison of bulk period L_0 of lamellae (L) and cylinders (C) formed by the DPDC model of linear DBCs obtained from molecular simulations and SCF calculations in previous work by our group, where N=10, $b/\sigma = \sqrt{3}/2$, and N/κ=50π.

* This data point is obtained from the pressure-tensor approach by us and corrects that reported in Ref. 1.

Phase	f_A	$\rho_0\sigma^3$	χN	L_0/σ	$L_{0,SCF}/L_0$	Ref.
L	1/2	3	30π	6.487±0.005	1.064	1
L	1/2	5	20π	6.10±0.01	1.043	1
L	2/5	3	30π	6.487±0.008	1.062	1
L	2/5	3	25π	6.2256±0.0003	1.068	11
L	2/5	5	20π	6.106±0.004	1.039	*
C	3/10	3	30π	6.814±0.005	1.066	30
C	3/10	5	20π	6.43±0.01	1.038	1

Similarly, from the results obtained by our group in previous work[1,11,30], Table 2 compares L_0^{SCF} with L_0 of L and hexagonally packed cylinders (C) formed by the DPDC model of DBCs obtained from Monte Carlo simulations in a rectangular prism simulation box of variable lengths at fixed volume[1] and from DPD simulations using the pressure tensor[11,30]. Combining the two

Table 3. Parameter-free comparison of the differences in excess Helmholtz free energy and its components from the corresponding homopolymer melts (*i.e.*, at χN=0) for ordered phases formed by the DPDC model of ABC stars obtained from LD simulations and SCF calculations, where the system # refers to that in Table 1, $\rho_0\sigma^3$=3, $b/\sigma=\sqrt{3}/2$, and N/κ=50.

#	L/σ	LD results	SCF results
1	8.6772	$\beta\Delta f_c$=4.494±0.029, $\beta\Delta u_c^{\mathrm{nb}}$=2.5638±0.0016, $\Delta s_c/k_B$=−1.930±0.029, $\beta\Delta PN/\rho_0$=4.564±0.005, $\beta\Delta\mu$=9.057±0.029	$\beta\Delta f_c$=9.238, $\beta\Delta u_c^{\mathrm{nb}}$=4.0418, $\Delta s_c/k_B$=−5.196, $\beta\Delta PN/\rho_0$=4.042, $\beta\Delta\mu$=13.279
2	7.6013	$\beta\Delta f_c$=5.906±0.109, $\beta\Delta u_c^{\mathrm{nb}}$=3.176±0.004, $\Delta s_c/k_B$=−2.730±0.109, $\beta\Delta PN/\rho_0$=6.1224±0.0081, $\beta\Delta\mu$=12.029±0.109	$\beta\Delta f_c$=11.799, $\beta\Delta u_c^{\mathrm{nb}}$=3.557, $\Delta s_c/k_B$=−8.242, $\beta\Delta PN/\rho_0$=3.5574, $\beta\Delta\mu$=15.357
3	8.9458	$\beta\Delta f_c$=4.115±0.050, $\beta\Delta u_c^{\mathrm{nb}}$=2.6985±0.0025, $\Delta s_c/k_B$=−1.417±0.050, $\beta\Delta PN/\rho_0$=4.8895±0.0080, $\beta\Delta\mu$=9.005±0.050	$\beta\Delta f_c$=9.170, $\beta\Delta u_c^{\mathrm{nb}}$=4.0383, $\Delta s_c/k_B$=−5.132, $\beta\Delta PN/\rho_0$=4.0383, $\beta\Delta\mu$=13.208
4	7.6045	$\beta\Delta f_c$=7.043±0.071, $\beta\Delta u_c^{\mathrm{nb}}$=2.9079±0.0016, $\Delta s_c/k_B$=−4.135±0.071, $\beta\Delta PN/\rho_0$=5.4491±0.0053, $\beta\Delta\mu$=12.492±0.071	$\beta\Delta f_c$=12.109, $\beta\Delta u_c^{\mathrm{nb}}$=3.7247, $\Delta s_c/k_B$=−8.384, $\beta\Delta PN/\rho_0$=3.7247, $\beta\Delta\mu$=15.833
5	7.8793	$\beta\Delta f_c$=6.465±0.099, $\beta\Delta u_c^{\mathrm{nb}}$=2.9532±0.0016, $\Delta s_c/k_B$=−3.512±0.099, $\beta\Delta PN/\rho_0$=5.5780±0.0049, $\beta\Delta\mu$=12.043±0.098	$\beta\Delta f_c$=11.864, $\beta\Delta u_c^{\mathrm{nb}}$=3.7083, $\Delta s_c/k_B$=−8.156, $\beta\Delta PN/\rho_0$=3.7083, $\beta\Delta\mu$=15.572

tables, we see that $L_0^{SCF} > L_0$ in all cases and SCF theory overestimates the bulk period of an ordered structure by about 4~9%.

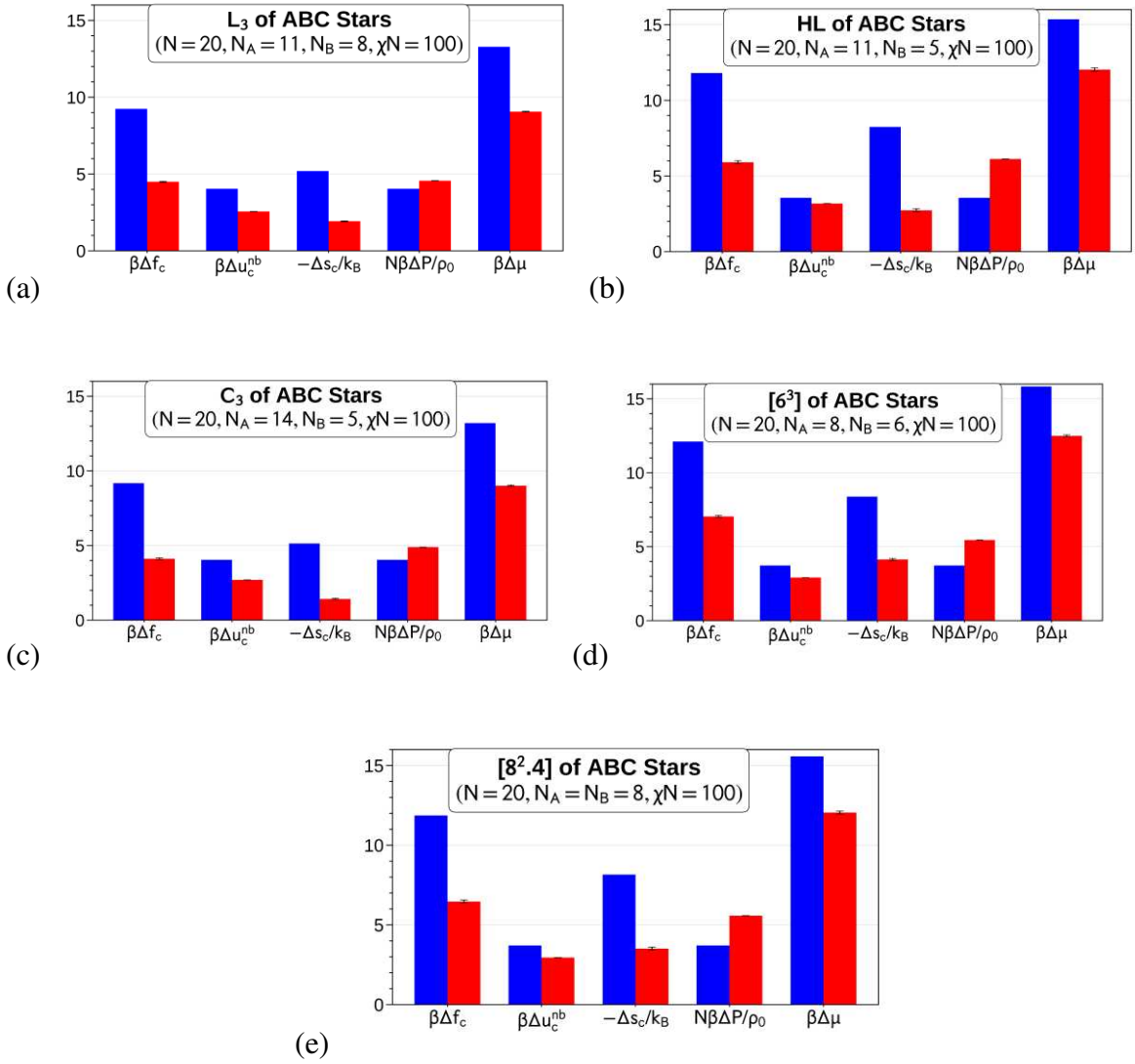

Figure 8. Parameter-free comparison of the differences in excess Helmholtz free energy and its components from the corresponding homopolymer melts (*i.e.*, at χN=0) for ordered phases (a) L_3, (b) HL, (c) C_3, (d) [6^3], and (e) [8^2,4] formed by the DPDC model of ABC stars of N=20 at χN=100 obtained from LD simulations and SCF calculations.

Table 3 and Figure 8 compare Δu_c^{nb}, ΔP, $\Delta\mu$, Δf_c, and Δs_c obtained from our LD simulations with the SCF predictions at the same period L close to the estimated L_0 for each system listed in Table

1; note that $\beta\Delta u_{c,\mathrm{SCF}}^{\mathrm{nb}} = \beta\Delta P_{\mathrm{SCF}} N/\rho_0$. We took the differences in excess Helmholtz free energy and its components from the corresponding homopolymer melts at χN=0, which is treated by SCF theory as a system of ideal chains due to its approximation.

We see that SCF theory overestimates the changes in f_c, u_c^{nb} and μ, and underestimates those in s_c and P for all the five structures formed by ABC stars, although there are some quantitative differences as expected. Since the system fluctuations tend to increase the mixing of different types of segments (thus increasing $\beta\Delta u_{c,\chi}^{\mathrm{nb}}$) but decreases the deviation of total segment volume fraction from 1 (thus decreasing $\beta\Delta u_{c,\kappa}^{\mathrm{nb}}$), the latter effect outweighs the former.

3.2 Relative Stability of Frank-Kasper Phases in DPDC Diblock Copolymer Melts

3.2.1 Numerical Accuracy of SCF Calculations

Before comparing the thermodynamic quantities of the Frank-Kasper (FK) phases, the numerical accuracy of the SCF calculations was checked. This step is important because the differences in the dimensionless Helmholtz free energy per chain, βf_c, among FK phases are small. Therefore, the SCF equations and the unit-cell optimization equations must be converged tightly enough so that the observed free-energy ordering is not caused by numerical error.

Previous SCF studies[19] used this same approach, where the numerical parameters were selected to obtain an accuracy in βf_c better than 10^{-5} at $\chi N = 40$ for the standard model. For the DPDC model the SCF equations were solved with $\epsilon_0 = 10^{-10}$, and the spatial discretization parameter $m = 64$ gave $\Delta(m) \equiv |\beta f_c(m) - \beta f_c(m = 128)| < 10^{-8}$ for the tested cases at $\chi N = 40$. These previous calculations provide useful accuracy standards for comparing small free-energy differences among ordered phases.

In the present work, the SCF calculations of 12 FK structures were performed for the DPDC model at $N = 20$, $f_A = 0.25$, $\epsilon = 4$, and $N/\kappa = 50$, with χN varied from 25 to 40. Because these structures have different unit-cell symmetries and different unit-cell aspect ratios, the grid settings are different from previous work. Instead, the spatial resolution was chosen separately for the present calculations by increasing the grid density until the SCF solution and the minimized free energy were satisfactory.

For each phase, the SCF equations and the unit-cell optimization equations were solved until the PSCF+ convergence criterion (10^{-6}) was satisfied[2]. The spatial discretization was then checked by repeating representative calculations using finer grids. A grid was considered satisfactory when further refinement produced a change in the minimized βf_c smaller than the convergence criterion.

This accuracy check is especially important for phases that are close in free energy. In the present calculations, A15 and H are the two closest phases to the reference σ phase, while several higher-free-energy phases, such as C14, C15, and the layered structures, become close to each other at large χN. Overall, the numerical checks confirm that the SCF calculations are sufficiently accurate for comparing the relative free energies, internal energies, and entropic contributions of the FK phases considered in this work.

3.2.2 Helmholtz Free Energy and Its Components

Figure 11 shows the dimensionless Helmholtz free energy per chain and its energetic and entropic contributions for the FK phases considered in this work. The calculations were performed for neat conformationally asymmetric diblock copolymer melts described by the DPDC model at $N = 20$, $f_A = 0.25$, $\epsilon = 4$, and $N/\kappa = 50$, with χN varied from 25 to 40. The σ phase was used as the reference phase. Thus, for a phase X, the relative Helmholtz free energy is

defined as $\Delta(\beta f_c)^{\mathrm{X}} = \beta f_c^{\mathrm{X}} - \beta f_c^{\sigma}$. The phases considered include 12 FK phases, namely A15, σ, H, Z, pσ, C14, C15, zra-d, 6-layers, 8-layers, 9-layers, and 10-layers structures shown in Figures 9 and 10.

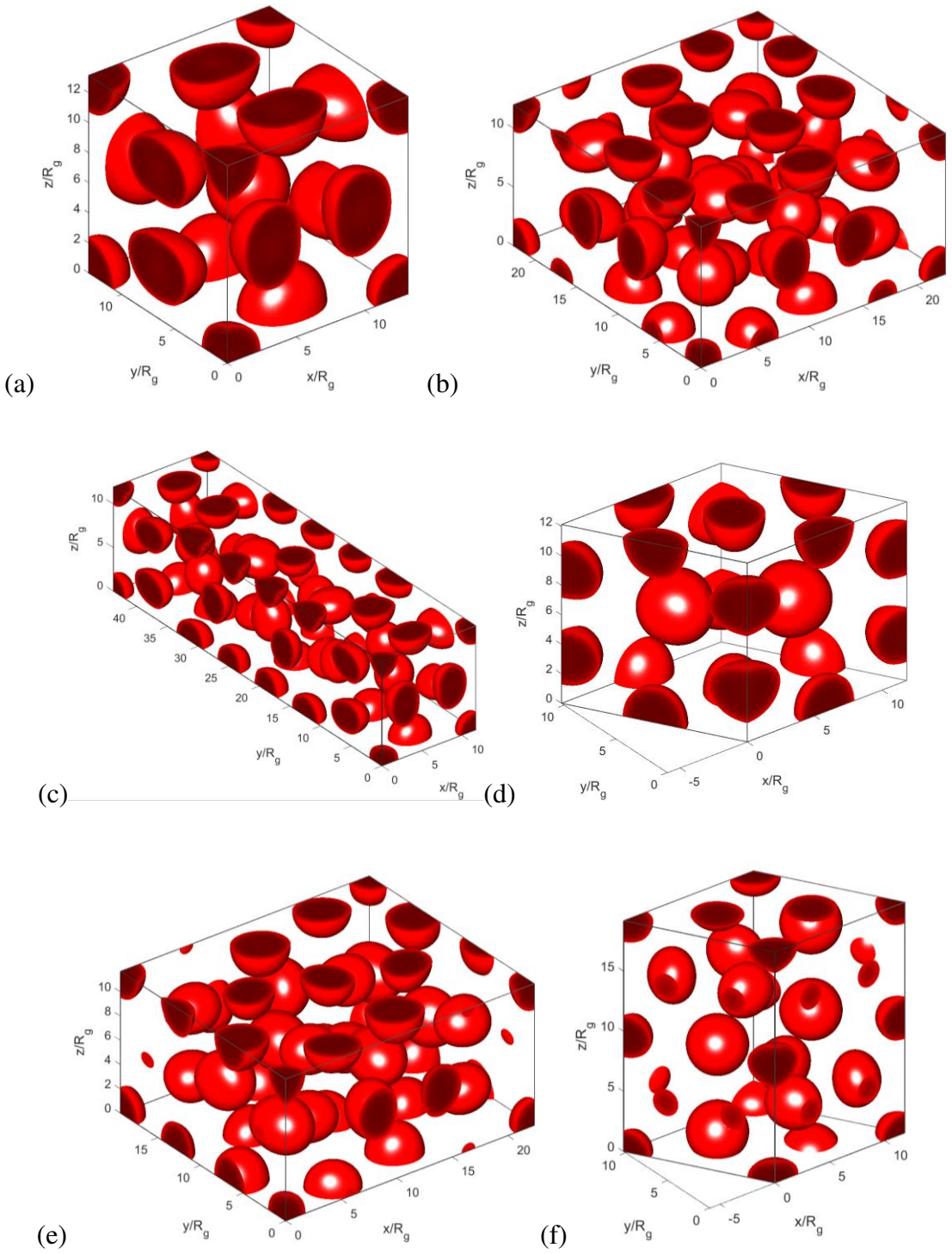

Figure 9. MATLAB visualizations of the converged SCF fields for (a) A15, (b) σ, (c) H, (d) Z, (e) pσ, and (f) C14 phases.

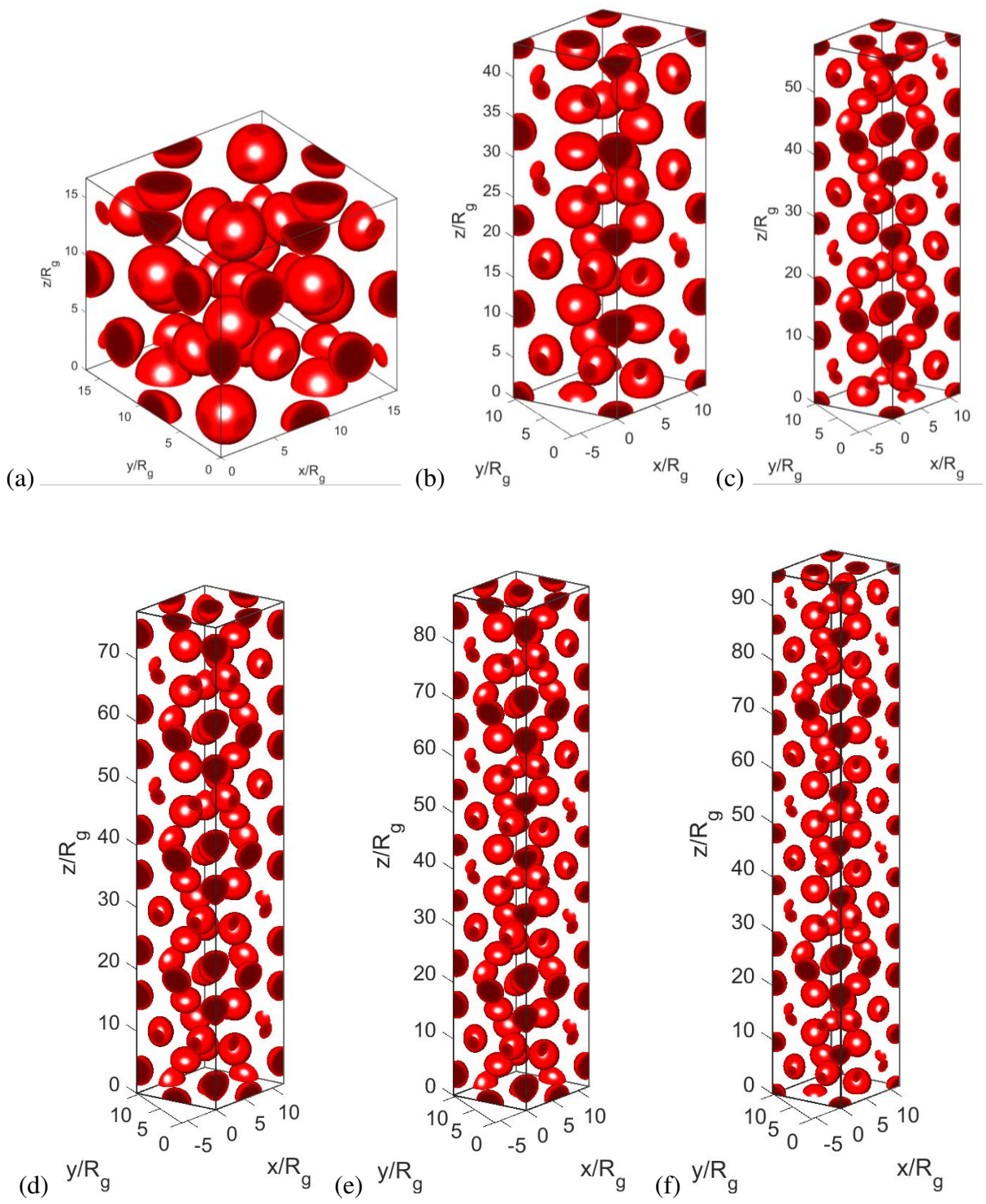

Figure 10. MATLAB visualizations of the converged SCF fields for (a) C15, (b) zra-d, (c) 6-layers, (d) 8-layers, (e) 9-layers, and (f) 10-layers phases.

Figure 11 (a) shows that σ has the lowest Helmholtz free energy among all FK phases considered over the full range $\chi N = 25 - 40$. All other FK structures considered here have positive $\Delta(\beta f_c)$, indicating that they are less stable than σ. Among the non-σ phases, A15 is the closest competitor throughout the entire χN range. Its relative free energy decreases from 3.66×10^{-4} at $\chi N = 25$ to 1.95×10^{-4} at $\chi N = 40$, showing that A15 becomes closer to σ as the segregation strength increases. H is the second closest phase to σ, with $\Delta(\beta f_c)$ increasing slightly from 3.92×10^{-4} to 4.70×10^{-4} over the same range. Therefore, the free-energy gap between A15 and H increases with increasing χN.

The remaining phases are substantially higher in free energy. At low χN, pσ, Z, and zra-d form an intermediate group with $\Delta(\beta f_c)$ values on the order of 10^{-3}. At $\chi N = 25$, their relative free energies are 1.24×10^{-3}, 1.31×10^{-3}, and 1.31×10^{-3}, respectively. Their ordering changes slightly with increasing χN: Z becomes lower in free energy than pσ above $\chi N \approx 27.2$, while zra-d becomes nearly degenerate with pσ near $\chi N = 40$.

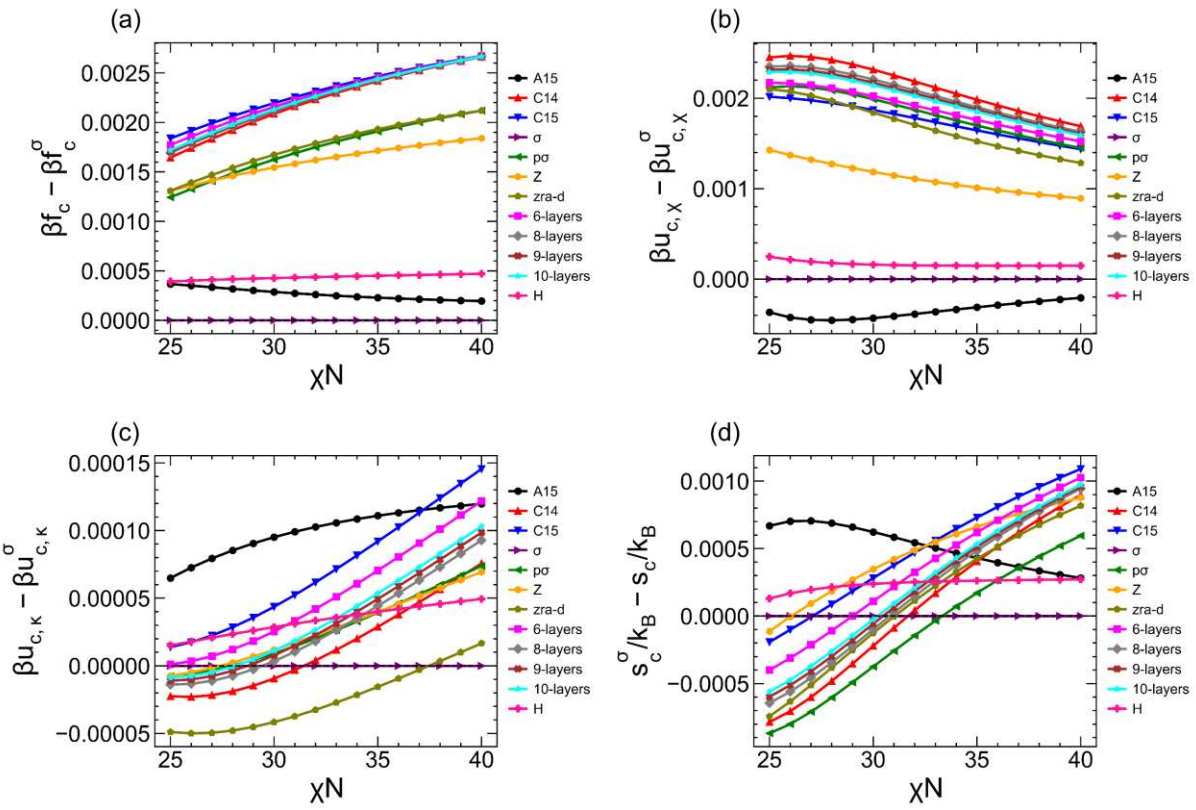

Figure 11. Comparisons of (a) the dimensionless Helmholtz free energies per chain, $\beta f_c - \beta f_c^{\sigma}$, (b) the dimensionless internal energies per chain due to the *A*–*B* repulsion $\beta u_{c,\chi} - \beta u_{c,\chi}^{\sigma}$ and (c) those due to the system compressibility $\beta u_{c,\kappa} - \beta u_{c,\kappa}^{\sigma}$, and (d) the dimensionless entropies per chain $s_c^{\sigma}/k_B - s_c/k_B$ of FK phases calculated using PSCF+ for neat conformationally asymmetric diblock copolymer melts described by the DPDC model at $N = 20$, $f_A = 0.25$, $\epsilon = 4$, and $N/\kappa = 50$, with the σ phase taken as a reference.

C14, C15, and the layered structures are higher in free energy than A15, H, Z, pσ, and zra-d over most of the range, becoming very close to each other at larger χN. For example, at $\chi N = 40$, their relative free energies all fall between 2.66×10^{-3} and 2.67×10^{-3}.

Figures 11 (b) and (c) decompose the internal energy into the *A*–*B* repulsion contribution and the compressibility contribution, showing $\Delta(\beta u_{c,\chi})^{\mathrm{X}} = \beta u_{c,\chi}^{\mathrm{X}} - \beta u_{c,\chi}^{\sigma}$ and $\Delta(\beta u_{c,\kappa})^{\mathrm{X}} = \beta u_{c,\kappa}^{\mathrm{X}} - \beta u_{c,\kappa}^{\sigma}$, respectively.

Most phases have positive $\Delta(\beta u_{c,\chi})$ since their *A*–*B* repulsion energy is larger than that of σ. This is one reason why their total free energies are higher. A15 is the only phase with a slightly lower *A*–*B* repulsion energy than σ throughout the entire range, with $\Delta(\beta u_{c,\chi})$ changing from -3.68×10^{-4} at $\chi N = 25$ to -2.07×10^{-4} at $\chi N = 40$. This favorable *A*–*B* repulsion contribution is one reason A15 is the closest competitor to σ. However, A15 remains higher in total free energy because its favorable *A*–*B* repulsion energy is offset by positive compressibility and entropic contributions.

For the other phases, the *A*–*B* repulsion contribution is positive over the full range. The phases in the high-free-energy group, including C14, C15, and the layered structures, have relatively large positive $\Delta(\beta u_{c,\chi})$. These values decrease with increasing χN, but they remain positive at $\chi N = 40$. H has only a small positive *A*–*B* repulsion contribution relative to σ, which is consistent with its position as the second closest non-σ phase in total free energy. Z has a lower *A*–*B* repulsion contribution than pσ and zra-d over much of the range, which contributes to its lower free energy at larger χN.

The compressibility contribution in Figure 11 (c) is much smaller than the *A*–*B* repulsion and entropic contributions for most phases. Over the full range studied, $\Delta(\beta u_{c,\kappa})$ remains on the order of 10^{-4} or smaller for all phases. This shows that the relative energetic differences among the FK phases are dominated mainly by the *A*–*B* repulsion term rather than by the compressibility term.

Figure 11 (d) shows the entropic contribution to the relative free energy, $\frac{s_c^{\sigma}}{k_B} - \frac{s_c^{\mathrm{X}}}{k_B}$. With this sign convention, the total relative free energy can be written as

$$\Delta(\beta f_c)^{\mathrm{X}} = \Delta\left(\beta u_{c,\chi}\right)^{\mathrm{X}} + \Delta\left(\beta u_{c,\kappa}\right)^{\mathrm{X}} + \left(\frac{s_c^{\sigma}}{k_B} - \frac{s_c^{\mathrm{X}}}{k_B}\right).$$

Thus, a positive value in Figure 11 (d) corresponds to an entropic penalty relative to σ, while a negative value corresponds to an entropic advantage relative to σ.

A15 illustrates the energy-entropy balance clearly. Although its *A*–*B* repulsion energy is lower than that of σ, it has positive entropic and compressibility contributions. The entropic contribution decreases with increasing χN, from 6.69×10^{-4} at $\chi N = 25$ to 2.82×10^{-4} at $\chi N = 40$, which leads to the decreasing free-energy gap between A15 and σ. In contrast, H has both a small positive *A*–*B* repulsion contribution and a small positive entropic contribution, giving a relative free energy that remains low but slowly increases with χN.

For most of the higher-free-energy phases, the entropic contribution is negative at low χN, partially compensating their unfavorable *A*–*B* repulsion energy. As χN increases, this entropic contribution becomes positive for most phases, adding to their free-energy penalty relative to σ. This change is especially visible for C14, C15, pσ, Z, zra-d, and the layered structures. Therefore, the increase in their relative free energies with increasing χN is caused not only by the internal-energy contribution but also by the loss of entropic advantage at larger segregation strength.

Overall, the thermodynamic decomposition shows that σ remains the lowest-free-energy FK phase among all structures considered in this work. A15 is the closest competitor, followed by H. The additional FK structures included in this work do not become competitive with the three lowest-free-energy phases σ, A15, and H over $\chi N = 25 - 40$. The layered structures and zra-d

do not change the main stability picture. They remain higher in free energy than the lowest phases, although several of them become nearly degenerate with C14 and C15 at high χN.

3.2.3 Average Coordination Number

The thermodynamic trends can also be related to the average coordination number $\bar{z}$ of the Wigner-Seitz polyhedra in each FK structure. The average coordination number is a purely geometric quantity defined from the numbers of Z12, Z14, Z15, and Z16 polyhedra in the unit cell. Previous FK stability analysis[19] showed that the variations of the βf_c- and βu_c-curves are clearly correlated with $\bar{z}$. In particular, FK phases having the same $\bar{z}$ tend to show nearly parallel free-energy and internal-energy curves, while the curve variations for phases with different $\bar{z}$ follow the same increasing or decreasing order as their $\bar{z}$ values.

Table 4. Number of Wigner-Seitz polyhedra n_z having coordination number z (= 12, 14, 15, and 16) and average coordination number $\bar{z}$ of the FK phases studied in this work.

Phase	n_{12}	n_{14}	n_{15}	n_{16}	$\bar{z}$
A15	2	6	0	0	13.5
σ	10	16	4	0	13.466
H	10	16	4	0	13.466
Z	3	2	2	0	13.428
pσ	14	4	4	4	13.384
zra-d	14	4	4	4	13.384
C14	8	0	0	4	13.333
C15	16	0	0	8	13.333
6-layers	24	0	0	12	13.333
8-layers	32	0	0	16	13.333
9-layers	36	0	0	18	13.333
10-layers	40	0	0	20	13.333

A similar qualitative trend is observed in the present DPDC calculations. Table 4 lists the $\bar{z}$ data[29] for all of the 12 considered FK phases. C14, C15, and the layered structures form a high-free-energy group whose $\Delta(\beta f_c)$ curves become nearly parallel and close to each other, especially at large χN. In addition, pσ and zra-d form a separate group showing the same trend, while H is almost parallel to σ accordingly. Therefore, the average coordination number provides a useful geometric way to organize the thermodynamic trends among FK phases. However, $\bar{z}$ alone does not uniquely determine the stable phase.

4. SUMMARY

In this thesis, the dissipative particle dynamics chain (DPDC) model was used to study ordered phases formed by block copolymer systems. The work contains two main parts. In the first part, Langevin dynamics (LD) simulations and self-consistent field (SCF) calculations were used to study ordered phases formed by ABC miktoarm star terpolymers. In the second part, SCF calculations were used to analyze the relative stability of Frank-Kasper (FK) phases in neat conformationally asymmetric diblock copolymer melts.

For the ABC star terpolymers, LD simulation parameters were first examined to ensure reliable sampling. The timestep was selected by comparing ensemble-averaged quantities from LD simulations with exact values. A timestep of $\delta t = 0.01\tau$ was used in the subsequent simulations. Each simulation was divided into a pilot run and a production run. The pilot run was used to determine the equilibration time, estimate statistical inefficiency, and choose a sampling interval for the production run so that the collected samples were nearly uncorrelated.

Finite-size effects were then examined because the periodic simulation box restricts the allowed period and orientation of ordered structures. For various ordered phases, thermodynamic quantities such as the non-bonded internal energy, pressure, excess chemical potential, and Helmholtz free energy were compared as functions of inverse system volume. The results showed that finite-size effects became small when two periods of the ordered structure were included. Therefore, two-period simulation boxes were used for the subsequent ABC-star calculations except for C_3, which showed multiple cylinder orientations in the simulation box.

The bulk periods of 5 ABC star ordered phases were determined from the pressure tensor[11]. The phases studied include three-layer lamellae L_3, hierarchical lamellae HL, core-shell cylinders C_3, the $[6^3]$ phase, and the $[8^2.4]$ phase. For each phase, the pressure-tensor anisotropy was calculated as a function of the period *L*, and the bulk period was estimated from a parabolic fit to the lowest three data points. These LD bulk periods were then compared with the corresponding SCF results obtained using PSCF+. Since the LD simulations and SCF calculations used the same DPDC model, the comparison was parameter-free.

The LD-SCF comparison showed that SCF theory overestimates the bulk period of the ordered ABC star phases by 4-9 percent, which is consistent with previous comparisons for block copolymer systems. The comparison of thermodynamic quantities showed that SCF theory overestimates the changes in excess Helmholtz free energy, non-bonded internal energy, and excess chemical potential from homopolymer melts, while it underestimates the corresponding changes in entropy and pressure. These differences are attributed to the mean-field approximation in SCF theory, which neglects fluctuations and correlations that are considered in LD simulations.

For the FK phases, SCF calculations were performed for neat conformationally asymmetric diblock copolymer melts described by the DPDC model. The parameter set was $N = 20$, $f_A = 0.25$, $\epsilon = 4$, and $N/\kappa = 50$, with χN varied from 25 to 40. The phases considered include the 12 FK phases: A15, σ, H, Z, pσ, C14, C15, 10-layers, 9-layers, 8-layers, 6-layers, and zra-d structures.

Before comparing the FK phase thermodynamics, the numerical accuracy of the SCF calculations was checked. This step is important because the free-energy differences among FK

phases are small. For each phase, the SCF equations and unit-cell optimization equations were solved until the PSCF+ convergence criterion was satisfied. The spatial resolution was selected by refining the grid until the minimized free energy was sufficiently accurate.

The relative stability of the FK phases was analyzed using the σ phase as the reference. The relative Helmholtz free energy, A–B repulsion contribution, compressibility contribution, and entropic contribution were plotted as functions of χN. Among all FK phases considered, the σ phase had the lowest Helmholtz free energy over the full range $\chi N = 25$–40. A15 was the closest competing phase, and its free-energy difference relative to σ decreased as χN increased. H was the next closest phase, with a relative free energy that increased slightly over the same range.

The decomposition of the relative free energy showed that FK phase stability is controlled mainly by the A–B repulsion. For most phases, the A–B repulsion contribution was higher than that of σ, which contributed to their higher total free energies. A15 had a slightly lower A–B repulsion energy than σ, but this advantage was balanced by positive compressibility and entropic contributions. The compressibility contribution was generally smaller than the A–B repulsion and entropy contributions, indicating that the main competition among the FK phases comes from energy-entropy balance rather than compressibility.

The average coordination number $\bar{z}$ was also observed as a geometric measure for organizing the FK thermodynamic trends. Consistent with previous FK stability analysis[19], phases with the same $\bar{z}$ show similar variations in their free-energy and internal-energy curves. In particular, C14, C15, and the layered structures display nearly parallel trends and become very close to each other at large χN. A similar correlation is observed for zra-d and pσ, which have the same $\bar{z}$, and

for σ and H, which also share the same $\bar{z}$. Thus, $\bar{z}$ is useful for describing the relationship between FK geometry and thermodynamic trends, although it is not alone sufficient to determine the stability.

Overall, this thesis demonstrates how the DPDC model can be used consistently in both particle-based simulations and SCF calculations to study ordered block copolymer phases. For ABC star terpolymers, the parameter-free LD-SCF comparison provides insight into finite-size effects, bulk-period determination, and the influence of fluctuations and correlations. For FK phases, the SCF calculations extend previous thermodynamic stability analyses to the DPDC model and to additional FK structures. Together, these results contribute to a more detailed understanding of how molecular architecture, finite-size effects, and mean-field thermodynamics influence the stability of complex ordered phases in block copolymer systems.

5. FUTURE WORK

One of the possible directions that can be pursued to extend the current work is to analyze how different Wigner-Seitz polyhedra contribute to the free energy or internal energy. Thus, the internal-energy-weighted and Helmholtz-free-energy-weighted average coordination numbers $\bar{z}_u$ and $\bar{z}_f$ calculations for the FK phases studied would allow a more direct comparison between the local packing geometry and the energetic and free-energy contributions of each phase. Applying this analysis to the DPDC model would also make it possible to test whether the correlations observed in previous FK stability studies[19] remain valid for compressible discrete-chain melts with finite-range DPD interactions. Moreover, the stability of the studied phases formed by ABC stars is another direction to extend the LD-SCF comparison discussion using the same model.

REFERENCES

(1) Sandhu, P.; Zong, J.; Yang, D.; Wang, Q. On the Comparisons between Dissipative Particle Dynamics Simulations and Self-Consistent Field Calculations of Diblock Copolymer Microphase Separation. J. Chem. Phys. 2013, 138 (19), 194904.

(2) He, J.; Wang, Q. PSCF+: An Extended and Improved Open-Source Software Package for Polymer Self-Consistent Field Calculations. J. Chem. Theory Comput. 2025, 21 (19), 9879–9889.

(3) Zong, J.; Wang, Q. Fluctuation/Correlation Effects in Symmetric Diblock Copolymers: On the Order-Disorder Transition. J. Chem. Phys. 2013, 139 (12), 124907.

(4) Frenkel, D.; Smit, B. Understanding Molecular Simulation: From Algorithms to Applications, 2nd ed.; Academic Press: San Diego, 2002.

(5) Dotera, T.; Hatano, A. The Diagonal Bond Method: A New Lattice Polymer Model for Simulation Study of Block Copolymers. J. Chem. Phys. 1996, 105 (18), 8413–8427.

(6) Micka, U.; Binder, K. Unusual Finite Size Effects in the Monte Carlo Simulation of Microphase Formation of Block Copolymer Melts. Macro Theory & Simulations 1995, 4 (3), 419–447.

(7) He, J.; Wang, Q. Frank–Kasper Phases of Diblock Copolymer Melts: Self-Consistent Field Results of Two Commonly Used Models. Polymers 2024, 16 (3), 372.

(8) Gemma, T.; Hatano, A.; Dotera, T. Monte Carlo Simulations of the Morphology of ABC Star Polymers Using the Diagonal Bond Method. Macromolecules 2002, 35 (8), 3225–3237.

(9) Kirkensgaard, J. J. K. Striped Networks and Other Hierarchical Structures in AmBmCn (2m+n)-Miktoarm Star Terpolymer Melts. Phys. Rev. E 2012, 85 (3), 031802.

(10) Ueda, K.; Dotera, T.; Gemma, T. Photonic Band Structure Calculations of Two-Dimensional Archimedean Tiling Patterns. Phys. Rev. B 2007, 75 (19), 195122.

(11) Feng, Y.; Li, B.; Wang, Q. Finding the Bulk Periodicity of Lamellar and Cylindrical Structures Using the Pressure Tensor. Soft Matter 2022, 18 (26), 4923–4929.

(12) Lee, S.; Bluemle, M. J.; Bates, F. S. Discovery of a Frank-Kasper σ Phase in Sphere-Forming Block Copolymer Melts. Science 2010, 330 (6002), 349–353.

(13) Frank, F. C.; Kasper, J. S. Complex Alloy Structures Regarded as Sphere Packings. I. Definitions and Basic Principles. Acta Crystallogr. 1958, 11 (3), 184–190.

(14) Frank, F. C.; Kasper, J. S. Complex Alloy Structures Regarded as Sphere Packings. II. Analysis and Classification of Representative Structures. Acta Crystallogr. 1959, 12 (7), 483–499.

(15) Liu, X.-Y.; Yan, X.-Y.; Liu, Y.; Qu, H.; Wang, Y.; Wang, J.; Guo, Q.-Y.; Lei, H.; Li, X.-H.; Bian, F.; Cao, X.-Y.; Zhang, R.; Wang, Y.; Huang, M.; Lin, Z.; Meijer, E. W.; Aida, T.; Kong, X.; Cheng, S. Z. D. Self-Assembled Soft Alloy with Frank–Kasper Phases beyond Metals. Nat. Mater. 2024, 23 (4), 570–576.

(16) Bates, M. W.; Lequieu, J.; Barbon, S. M.; Lewis, R. M.; Delaney, K. T.; Anastasaki, A.; Hawker, C. J.; Fredrickson, G. H.; Bates, C. M. Stability of the A15 Phase in Diblock Copolymer Melts. Proc. Natl. Acad. Sci. U.S.A. 2019, 116 (27), 13194–13199.

(17) Schulze, M. W.; Lewis, R. M.; Lettow, J. H.; Hickey, R. J.; Gillard, T. M.; Hillmyer, M. A.; Bates, F. S. Conformational Asymmetry and Quasicrystal Approximants in Linear Diblock Copolymers. Phys. Rev. Lett. 2017, 118 (20), 207801.

(18) Xie, N.; Li, W.; Qiu, F.; Shi, A.-C. σ Phase Formed in Conformationally Asymmetric AB-Type Block Copolymers. ACS Macro Lett. 2014, 3 (9), 906–910.

(19) Zhuang, Z.; He, J.; Tang, J.; Wang, Q. Toward the Relative Stability of Frank–Kasper Phases Formed by Neat Diblock Copolymer Melts and Binary Blends. Macromolecules 2025, 58 (1), 415–423.

(20) He, J.; Wang, Q. Correction to "Frank–Kasper Phases of Diblock Copolymer Melts Studied with the DPD Model: SCF Results." Macromolecules 2024, 57 (3), 1399–1401.

(21) Helfand, E.; Tagami, Y. Theory of the Interface between Immiscible Polymers. II. J. Chem. Phys. 1972, 56 (7), 3592–3601.

(22) Helfand, E.; Tagami, Y. Theory of the Interface between Immiscible Polymers. J. Polym. Sci. B Polym. Lett. 1971, 9 (10), 741–746.

(23) Groot, R. D.; Warren, P. B. Dissipative Particle Dynamics: Bridging the Gap between Atomistic and Mesoscopic Simulation. J. Chem. Phys. 1997, 107 (11), 4423–4435.

(24) https://Glotzerlab.Engin.Umich.Edu/Hoomd-Blue/.

(25) Oliveira, F. L.; Luan, B.; Esteves, P. M.; Steiner, M.; Neumann Barros Ferreira, R. pyMSER─An Open-Source Library for Automatic Equilibration Detection in Molecular Simulations. J. Chem. Theory Comput. 2024, 20 (19), 8559–8568.

(26) Schultz, A. J.; Hall, C. K.; Genzer, J. Box Length Search Algorithm for Molecular Simulation of Systems Containing Periodic Structures. J. Chem. Phys. 2004, 120 (4), 2049–2055.

(27) Martínez-Veracoechea, F. J.; Escobedo, F. A. Simulation of the Gyroid Phase in Off-Lattice Models of Pure Diblock Copolymer Melts. J. Chem. Phys. 2006, 125 (10), 104907.

(28) Fredrickson, G. H. The Equilibrium Theory of Inhomogeneous Polymers, 1st ed.; Oxford, 2013.

(29) Dutour Sikirić, M.; Delgado-Friedrichs, O.; Deza, M. Space Fullerenes: A Computer Search for New Frank–Kasper Structures. Acta Crystallogr. Section A 2010, 66 (5), 602–615.

(30) Feng, Y.; Wu, J.; Li, B.; Wang, Q. Periodicity and Global Order Parameter of Hexagonally Packed Cylinders in a Periodic Box. Soft Matter 2022, 18 (14), 2750–2756.